Research Paper

Mitochondrial and ribosomal biogenesis are new hallmarks of stemness, oncometabolism and biomass accumulation in cancer: Mito-stemness and ribo-stemness features

Maria Peiris-Pagès [1], Béla Ozsvári [2], Federica Sotgia [2], Michael P. Lisanti [2]

[1]Clinical and Experimental Pharmacology, University of Manchester, Cancer Research UK, Manchester, United Kingdom

[2]Translational Medicine, School of Environment and Life Sciences, Biomedical Research Centre (BRC), University of Salford, Greater Manchester, United Kingdom

Correspondence to: Federica Sotgia, Michael P. Lisanti; **email:** fsotgia@gmail.com, michaelp.lisanti@gmail.com
Keywords: coculture, tumor microenvironment, proteomics, mito-stemness, ribo-stemness, mitochondria, protein synthesis, organelle biogenesis
Received: May 23, 2019 **Accepted:** June 20, 2019 **Published:** July 16, 2019

ABSTRACT

Using proteomics analysis, we previously compared MCF7 breast cancer cells grown as 3D tumor spheres, with the same cell line grown as monolayers. Our results indicated that during 3D anchorage-independent growth, the cellular machinery associated with i) mitochondrial biogenesis and ii) ribosomal biogenesis, were both significantly increased. Here, for simplicity, we refer to these two new oncogenic hallmarks as "mito-stemness" and "ribo-stemness" features. We have now applied this same type of strategy to begin to understand how fibroblasts and MCF7 breast cancer cells change their molecular phenotype, when they are co-cultured together. We have previously shown that MCF7-fibroblast co-cultures are a valuable model of resistance to apoptosis induced by hormonal therapies, such as Tamoxifen and Fulvestrant. Here, we directly show that these mixed co-cultures demonstrate the induction of mito-stemness and ribo-stemness features, likely reflecting a mechanism for cancer cells to increase their capacity for accumulating biomass. In accordance with the onset of a stem-like phenotype, KRT19 (keratin 19) was induced by ~6-fold during co-culture. KRT19 is a well-established epithelial CSC marker that is used clinically to identify metastatic breast cancer cells in sentinel lymph node biopsies. The potential molecular therapeutic targets that we identified by label-free proteomics of MCF7-fibroblast co-cultures were then independently validated using a bioinformatics approach. More specifically, we employed publically-available transcriptional profiling data derived from primary tumor samples from breast cancer patients, which were previously subjected to laser-capture micro-dissection, to physically separate breast cancer cells from adjacent tumor stroma. This allowed us to directly validate that the proteins up-regulated in this co-culture model were also transcriptionally elevated in patient-derived breast cancer cells *in vivo*. This powerful approach for target identification and translational validation, including the use of patient outcome data, can now be applied to other tumor types as well, to validate new therapeutic targets that are more clinically relevant, for patient benefit. Moreover, we discuss the therapeutic implications of these findings for new drug development, drug repurposing and Tamoxifen-resistance, to effectively target mito-stemness and ribo-stemness features in breast cancer patients. We also discuss the broad implications of this "organelle biogenesis" approach to cancer therapy.

INTRODUCTION

Cancer stem cells (CSCs) are now thought to be one of the major drivers behind treatment failure in many cancer types, including breast cancer [1]. As a consequence, residual CSCs, which are chemo-resistant and radio-resistant, result in tumor recurrence and distant metastasis, ultimately killing most cancer patients [2]. Therefore, there is an urgent need to understand what are the metabolic weak points within CSCs, to drive new drug discovery, for patient benefit. This requires new innovative approaches towards understanding "stemness" features and identifying specific metabolic targets in CSCs [3-5].

In order to identify new characteristic features of "stemness" in cancer cells, we previously compared the proteomic profiles of 3D-spheroid cultures of MCF7 breast cancer cells, with MCF7 monolayer cells, processed in parallel [6]. These 3D-spheroids were grown under anchorage-independent conditions and are also known as mammosphere cultures, which are highly enriched in CSCs and cancer progenitor cells [6]. Using this approach, we previously demonstrated that under these 3D growth conditions, MCF7 cells up-regulated the expression of >60 mitochondrial-related proteins and >80 proteins related to protein synthesis, including ribosomal biogenesis [6,7]. Moreover, we have shown that pharmacologically targeting protein synthesis and/or mitochondrial function are both indeed sufficient to eradicate CSCs [8-14].

Here, we refer to these characteristic proteomic changes as "mito-stemness" [15] and "ribo-stemness". We have now investigated whether these stemness features are also similarly up-regulated during the co-culture of MCF7 breast cancer cells with fibroblasts. Our current observations are consistent with the idea that MCF7-fibroblast co-cultures increase their biosynthetic cellular machinery, to expand their capacity to increase biomass. Therefore, "mito-stemness" and "ribo-stemness" features are actually oncogenic hallmarks of the ability and readiness of cancer cells to aggressively undergo biomass accumulation.

We also discuss the implications of our current findings for understanding and treating Tamoxifen-resistance, as we have previously validated that the MCF7-fibroblast co-culture system is a bonafide model of Tamoxifen- resistance [16], which includes a stromal micro- environment, making it perhaps more physiologically- relevant.

RESULTS

Unbiased proteomics analysis: identification of proteins up-regulated in MCF7-fibroblast co-cultures

Previously, we have demonstrated that cancer cells, grown in close proximity to fibroblasts, metabolically reprogram these fibroblasts towards a more catabolic state, via the induction of autophagy, mitophagy and glycolysis, as well as senescence [16-20]. Conversely, through this interaction, cancer cells undergo reciprocal metabolic reprogramming towards a more anabolic state, with the induction of mitochondrial biogenesis and oxidative metabolism [21,22]. This metabolic co-operation primarily benefits the cancer cells by providing nutrients to generate new biomass [17,18]. Unfortunately, most of the metabolic targets in this symbiotic process remain completely unknown.

Here, we developed a new approach to identify these potential therapeutic targets, via unbiased proteomics analysis. For this purpose, we used MCF7 cells, an ER(+) human breast cancer cell line, as a model system. These MCF7 cells were co-cultured with hTERT-BJ1 fibroblasts, in a cellular ratio of 1:1, for a short 3-day period. These MCF7-fibroblast co-cultures were then directly compared to a 1:1 protein mixture of MCF7 cells and hTERT-fibroblasts, that had not been co- cultured together, but were grown instead as homotypic mono-cultures (Figure 1).

To a first approximation, using proteomics, this approach should allow us to estimate and identify which proteins are increased during the co-culture process, relative to mono-cultures. Then, these protein candidates were compared with human breast cancer samples that had undergone laser-capture micro-dissection, to validate their relevant expression in human breast cancer cells *in vivo*. For this purpose, we used publicly-available transcriptional-profiling data (from N=28 breast cancer patients; See Materials and Methods). A diagram highlighting this work-flow is shown as Figure 2.

Previously, we have shown that mitochondrial biogenesis in MCF7 cells is induced when they are co- cultured with fibroblasts [21,22]. However, it remains unknown exactly which mitochondrial proteins are induced during co-culture. Therefore, we focused first on which mitochondrial proteins were increased during co-culture, based on this proteomics approach.

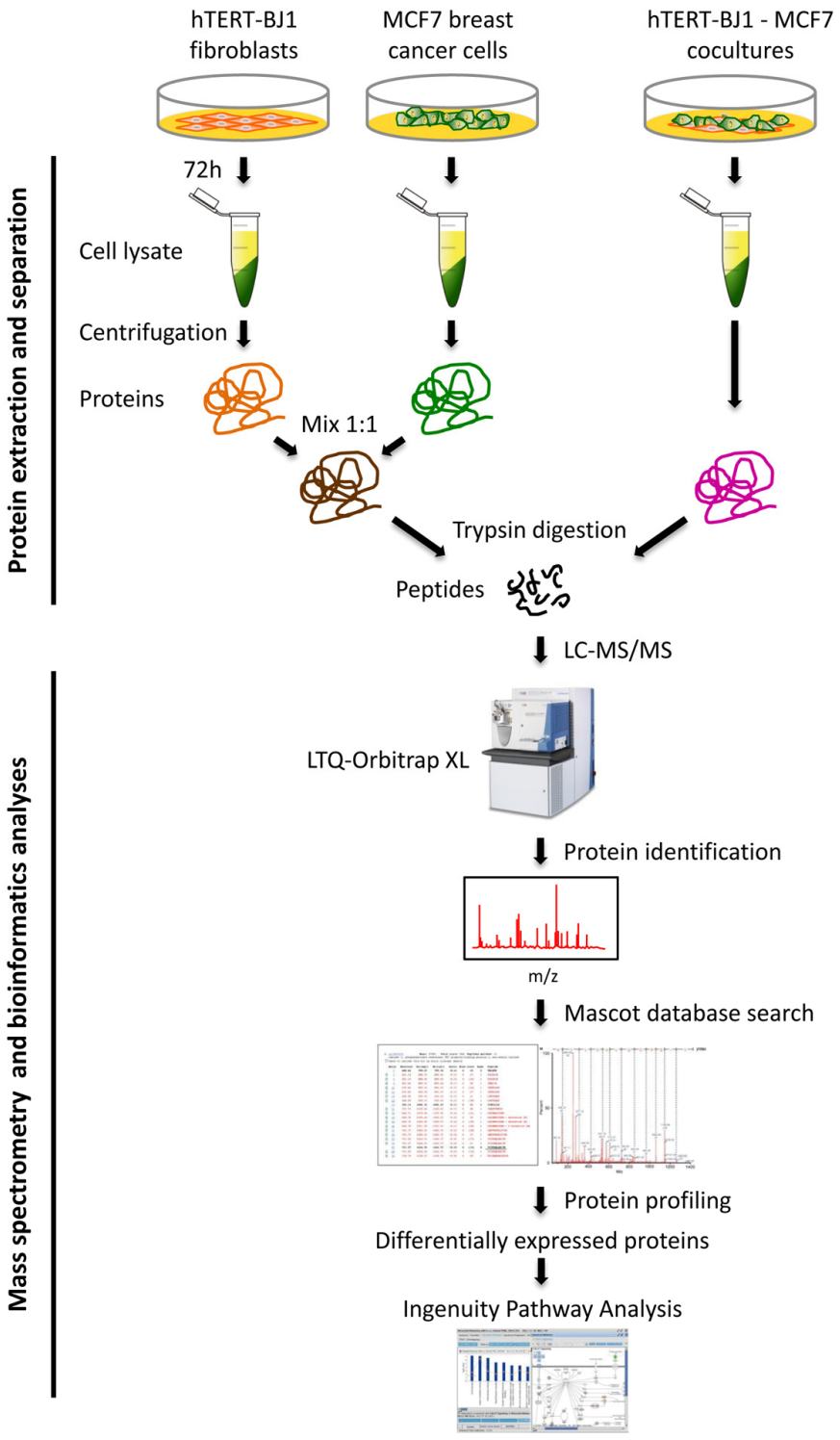

Figure 1. Schematic diagram summarizing the work-flow for MCF7-fibroblast co-culture studies and bioinformatics validation. Protein lysates were obtained from hTERT-BJ1 fibroblasts after 72 h co-culture with MCF7 breast cancer cells. Alternatively, protein lysates were obtained from hTERT-BJ1 fibroblasts and MCF7 cells cultured separately as monolayers and then mixed. Peptides obtained after trypsin digestion were analysed via LC-MS/MS on an LTQ- Orbitrap XL mass spectrometer. Label-free quantitative proteomics was used to detect changes in protein abundances across co-cultures and mixed cell population extracts. The proteomics data sets were further analyzed using Ingenuity Pathway Analysis. This co-culture approach is predicted to better simulate the fibroblast-rich local tumor micro-environment *in vivo*.

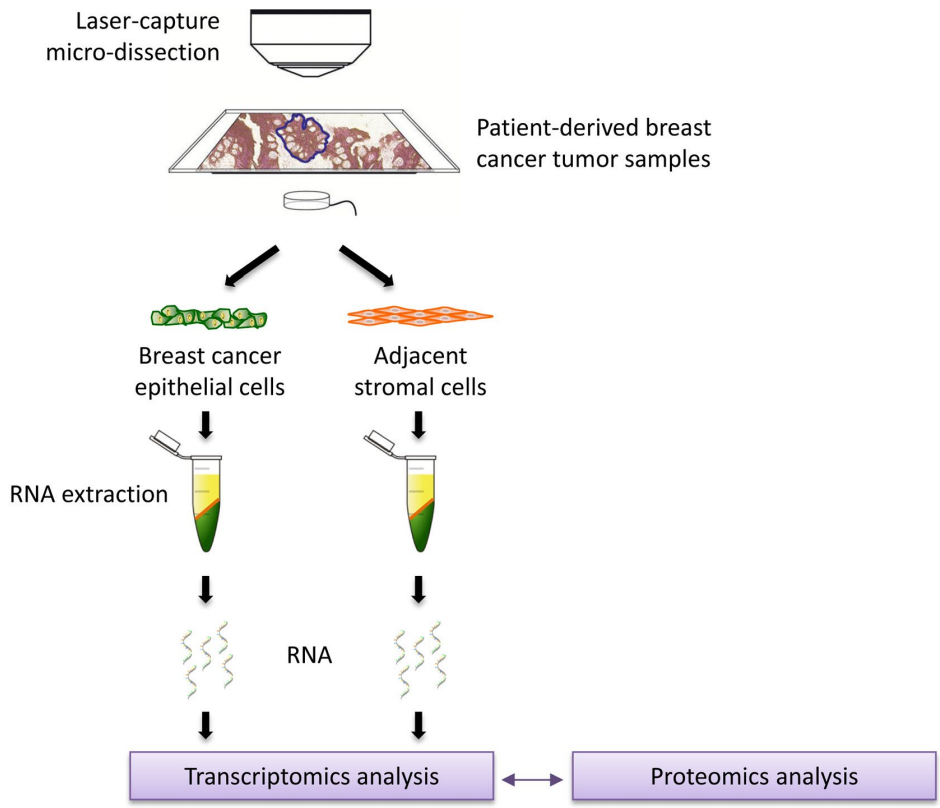

Figure 2. Schematic diagram summarizing the work-flow for validation studies with transcriptional profiling data from clinical samples. Data from N=28 patient-derived breast primary tumor samples, which have been subjected to laser-capture micro-dissection, were used for validation.

Supplementary Table 1 illustrates the 45 mitochondrial-related proteins that were found to be significantly up-regulated during the MCF7-fibroblast co-culture process. This list includes proteins that are involved in mitochondrial biogenesis and/or are part of the mitochondrial complexes I to V, as well as mito-chondrial chaperones, such as DNAJA3, HSPD1 and HSPA9, among others. Interestingly, NDUFAF2, a MYC-induced component of complex I [23], was infinitely up-regulated during co-culture. Interestingly, we have previously shown that the co-culture of MCF7 cells with fibroblasts confers Tamoxifen-resistance, that is reversible by treatment with Metformin, a complex I inhibitor [16]. Therefore, NDUFAF2 (a.k.a, Mimitin [23]) may be functionally conferring Tamoxifen-resistance during co-culture.

Since increased mitochondrial biogenesis is a hallmark of cancer stem cells (CSCs), known as "mito-stemess" [6-8,15], we next also looked for markers of protein synthesis [7], that is another hallmark of CSCs, which we now refer to here as "ribo-stemness". Supplementary Table 2 shows that 28 components of the large and small cellular ribosomal subunits were up-regulated during co-culture. More specifically, 18 components of the large 60S ribosome and 10 components of the small 40S ribosome were increased. Interestingly, RPL4 and RPS29 were infinitely increased during co-culture.

Consistent with these findings, protein-folding chaperones were also induced. Supplementary Table 3 lists 10 chaperones that were significantly increased during co-culture. These include members of the HSP90 and HSP70 families of chaperones, as well as others. Remarkably, HSP90AB1 was infinitely up-regulated.

Similarly, Supplementary Table 4 shows that proteins involved in mRNA translation initiation, polypeptide elongation, tRNA synthesis and amino acid uptake were all significantly up-regulated during co-culture. Overall, this includes 30 proteins in total. For example, EIF2S1, a translation initiation factor required for mRNA binding to ribosomes, was increased by nearly 300-fold.

Furthermore, other well-known markers of "stemness" and proliferation were increased, as shown in Supplementary Table 5. More specifically, MKI67 was

Table 1. Proteomics summary: key targets that were up-regulated by >100-fold in MCF7-fibroblast co-cultures.

Gene	Description	Fold-increase
1. Mitochondrial Proteins		
NDUFAF2	Mimitin, c-Myc-induced mitochondrial protein; B17.2L	Infinity
GPD2	Glycerol-3-phosphate dehydrogenase, mitochondrial	238.91
AIFM1	Apoptosis-inducing factor 1, mitochondrial	237.74
PRKDC	DNA-dependent protein kinase catalytic subunit	102.78
2. Ribosomal Proteins		
RPL4	60S ribosomal protein L4	Infinity
RPS29	40S ribosomal protein S29	Infinity
RPL15	60S ribosomal protein L15	2,238.12
RPL19	60S ribosomal protein L19	168.84
3. Chaperone and Translation initiation factors		
HSP90AB1	Heat Shock Protein 90kDa Alpha (Cytosolic), Class B Member 1	Infinity
EIF2S1	Eukaryotic translation initiation factor 2 subunit 1	291.47
4. Ribosomal RNA (rRNA) synthesis		
MKI67	Antigen KI-67	4,531.38

increased by >4,000-fold, while KRT19 and PCNA were increased by nearly 6-fold and 4-fold, respectively. The profound increase in MKI67 is more consistent with increased protein synthesis, rather than increased proliferation. Interestingly, MKI67 is expressed in all cycling cells, except for resting cells in the G0-phase and is specifically associated with ribosomal RNA (rRNA) synthesis and, thus, protein synthesis. This is consistent with our results presented in Supplementary Tables 2-4.

In this context, it is interesting to note that KRT19 is a well-established epithelial CSC marker that is used clinically to identify metastatic breast cancer cells in sentinel lymph node biopsies [24,25].

A summary of the proteins that were up-regulated by >100-fold is highlighted in Table 1. In conclusion, our current observations are consistent with the idea that MCF7-fibroblast co-cultures increase their biosynthetic cellular machinery (i.e., mitochondria and ribosomes), to expand their anabolic capacity to increase their biomass.

Ingenuity pathway analysis (IPA) of MCF7-fibroblast co-cultures

Differentially expressed proteins were also independently analyzed using Ingenuity Pathway Analysis (IPA), to identify altered canonical pathways and toxicity functions.

This analysis revealed that EIF2 signaling, which is crucial for protein synthesis, is a significantly activated canonical pathway in co-cultures, as compared to mono- cultures, as measured by a z-score

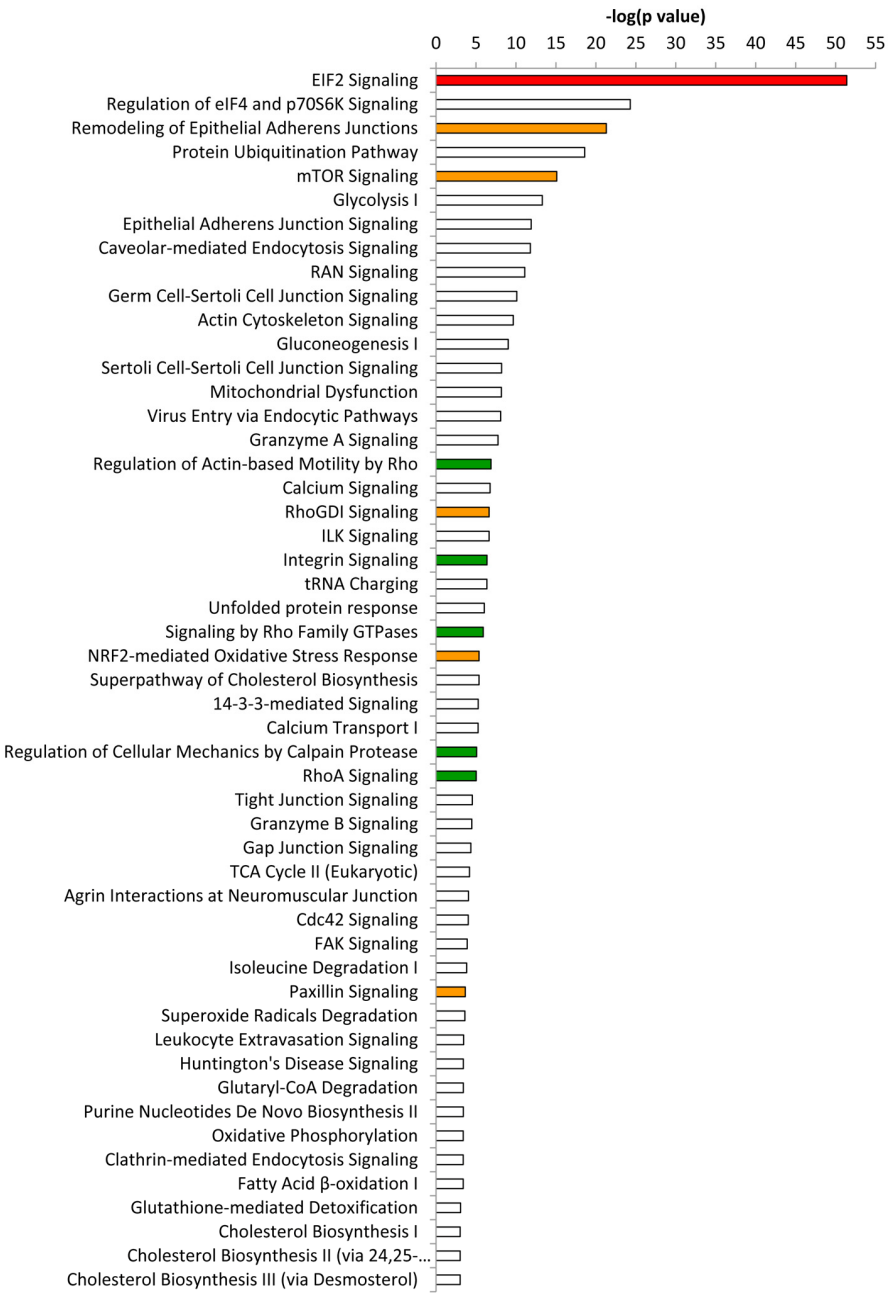

Figure 3. Ingenuity pathway analysis of differentially expressed proteins in co-cultures compared to mixed cell populations. Ingenuity Pathway Analysis (IPA) showed canonical pathways significantly altered ($p < 0.001$). The p value for each pathway is indicated by the bar and is expressed as -1 times the log of the p value. Red colored bars indicate a predicted significant activation of the pathway (z-score >2), whereas orange colored bars indicate a not significant activation (z-score between 0 and 2). **Green** bars indicate a not significant inhibition of the pathway (z-score between 0 and -2). White bars indicate that the pathway is altered, but it was not possible to predict whether it is activated nor inhibited.

> 2 (Figure 3). Other altered pathways and toxicity functions identified by IPA included mitochondrial dysfunction, NRF2- mediated oxidative stress, fatty acid metabolism, changes in mitochondrial membrane potential, HIF signaling, glutathione depletion, mitochondrial biogenesis, DNA-damage and fibrosis, among others (Figure 4). The observed similarity with renal injury appears to be related to an increase in oxidative stress and the resulting anti-oxidant response.

Overall, these results are consistent with the induction of "mito-stemness" and "ribo-stemness" features, during the co-culture process.

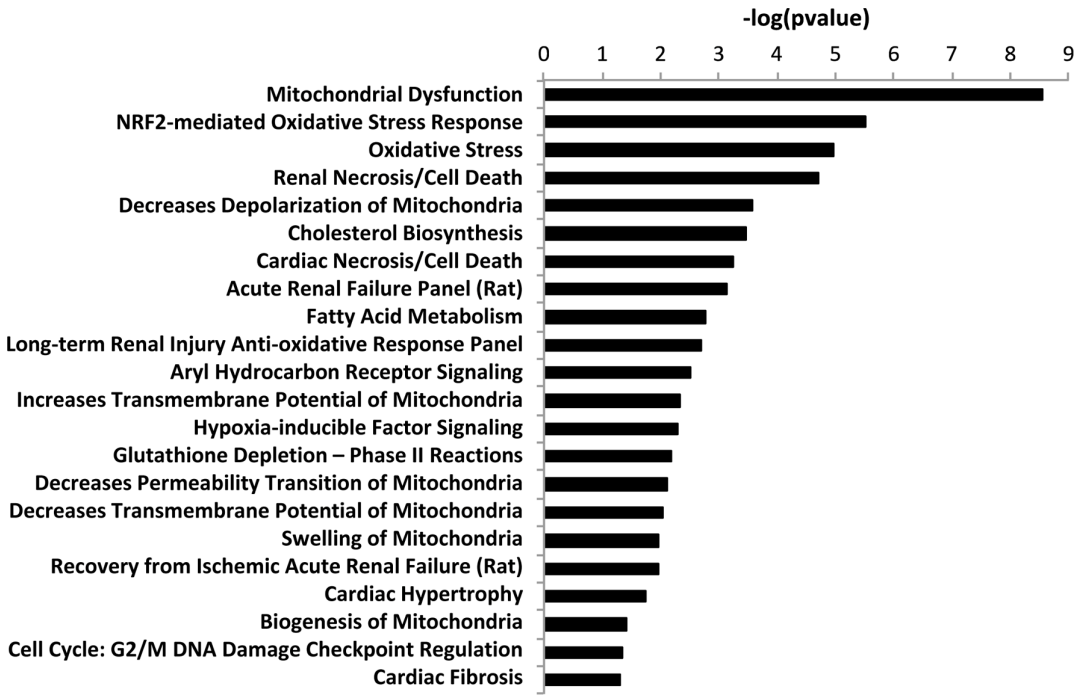

Figure 4. "Toxicity" effects of differentially expressed proteins in co-cultures versus monocultures. Ingenuity Pathway Analysis showed toxicity functions significantly enriched by the proteins differentially expressed in co-cultures ($p < 0.05$). The p value for each pathway is indicated by the bar and is expressed as -1 times the log of the p value.

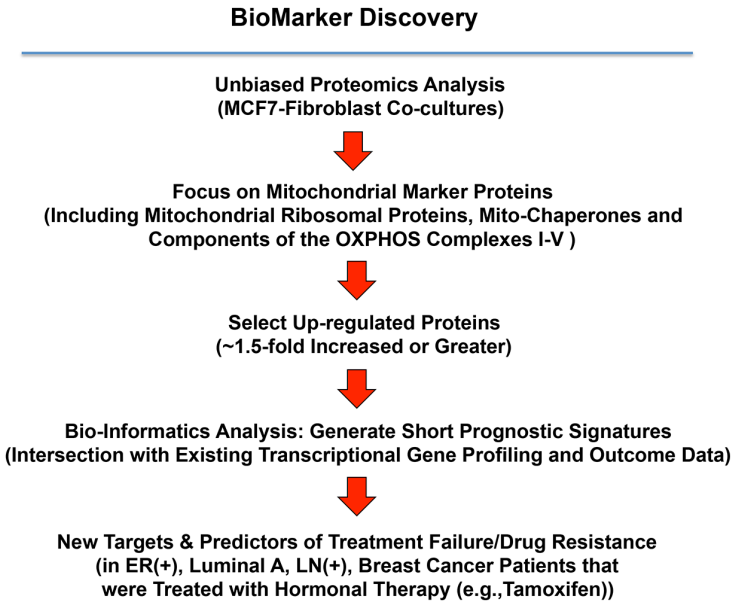

Figure 5. A proteomics-based approach to the development of new breast cancer companion diagnostics, for predicting Tamoxifen-resistance. For this analysis, data from the proteomics analysis of MCF7- fibroblast co-cultures was intersected with clinical outcome data. More specifically, the clinical population we focused included ER(+) patients, of the luminal A sub-type, that were lymph-node positive (LN(+)) at diagnosis, who were treated with Tamoxifen and followed over nearly 200 months. In this context, we ultimately evaluated the prognostic value of a mitochondrial signature for predicting tumor treatment failure (recurrence, metastasis or overall survival).

Table 2. Prognostic value of mitochondrial markers induced during metabolic symbiosis (MCF7-fibro) for tumor recurrence.

Gene Probe ID	Symbol	Hazard-Ratio (RFS)	Log-Rank Test
211662_s_at	VDAC2	3.96	6.70E-07
200807_s_at	HSPD1	3.46	1.30E-05
200806_s_at	HSPD1	2.34	0.005
203633_at	CPT1A	2.86	0.01
203634_s_at	CPT1A	2.32	0.025
202698_x_at	COX4I1	2.19	0.038
211971_s_at	LRPPRC	2.05	0.01
200657_at	SLC25A5	2.4	0.002
221235_s_at	TRAP1	1.77	0.048

RFS: recurrence-free survival.

Validating the clinical relevance of co-culture proteomics data, using patient-derived breast tumor samples

In order to directly validate the potential clinical relevance of our findings, we next used transcriptional profiling data derived from the analysis of N=28 breast cancer patients, which were previously subjected to laser-capture micro-dissection, to physically separate breast cancer cells from adjacent stromal cells [26].

Therefore, we intersected our proteomics data, with this clinical data set, and the levels of fold-upregulation observed in the epithelial cancer cell compartment (relative to the tumor stroma), and corresponding p-values derived from these clinical samples, are shown in Supplementary Tables 6 to 9.

Supplementary Table 6 shows that of the 45 mitochondrial proteins that were up-regulated during co-culture, 34 were also significantly increased by >1.75-fold in human breast cancer cells *in vivo*. Therefore, >75% of the mitochondrial proteins elevated during co-culture were transcriptionally increased in patient-derived breast cancer cells *in vivo*.

Similarly, Supplementary Table 7 highlights that of the 28 ribosomal proteins that were up-regulated during co-culture, 27 were significantly increased by >1.7-fold in human breast cancer cells *in vivo*. Thus, >96% of the ribosomal proteins elevated during co-culture were transcriptionally increased in human breast cancer cells *in vivo*.

In addition, Supplementary Table 8 illustrates that of the 10 chaperone proteins that were up-regulated during co-culture, 7 were significantly increased by >3.1-fold in human breast cancer cells *in vivo*. As such, 70% of the chaperone proteins increased during co-culture were also increased in human breast cancer cells.

Finally, Supplementary Table 9 shows that of the 30 proteins associated with mRNA translation initiation, polypeptide elongation, and tRNA synthesis, 19 were significantly increased by >1.7-fold in human breast cancer cells *in vivo*. As a result, >60% of these proteins were also increased in human breast cancer cells.

Such a high concordance rate, between i) in vitro proteomics data and ii) in vivo human breast cancer transcriptional mRNA data, clearly validates the translational significance of the MCF7-fibroblast co-culture system, as a model for studying human breast cancer.

Establishing new prognostic biomarkers and companion diagnostics for predicting tamoxifen-resistance, by exploiting proteomics data from MCF7-fibroblast co-cultures

We have previously shown that the co-culture of MCF7 cells with fibroblasts induces a Tamoxifen-resistance phenotype [16]. Therefore, to identify new potential biomarkers of Tamoxifen-resistance, here we intersected our proteomics data from MCF7-fibroblast co-cultures with publicly available transcriptional profiling data from the tumors of breast cancer patients that were treated with Tamoxifen, but did not receive any chemotherapy [27,28]. A schematic diagram summarizing this approach is shown in Figure 5.

Table 3. A 3-Gene mitochondrial signature for predicting treatment failure, due to tumor recurrence.

Gene Probe ID	Symbol	Hazard-Ratio (RFS)	Log-Rank Test
211662_s_at	VDAC2	3.96	6.70E-07
200807_s_at	HSPD1	3.46	1.30E-05
203633_at	CPT1A	2.86	0.01
Combined		5.52	7.30E-10

RFS: recurrence-free survival.

Table 4. A 3-Gene mitochondrial signature for predicting treatment failure, due to distant metastasis.

Gene Probe ID	Symbol	Hazard-Ratio (DMFS)	Log-Rank Test
211662_s_at	VDAC2	3.11	0.0004
200807_s_at	HSPD1	3.5	9.70E-05
203633_at	CPT1A	2.79	0.026
Combined		5.51	8.10E-07

DMFS: distant metastasis-free survival.

For this purpose, we selected high-risk patients that were lymph-node positive at diagnosis, and we focused on the luminal A subtype, which represents the most common form of ER(+) breast cancers (N = 152 patients). The results of this analysis are shown in Table 2. In this context, seven distinct mitochondrial genes, represented by 9 different gene probes, showed significant prognostic value, and were able to predict tumor recurrence.

In order to increase the prognostic power of these individual mitochondrial biomarkers, we next selected the most promising ones and used them to create a new mitochondrial gene signature. This new Mito-Signature contains only 3 key genes (HSPD1, VDAC2, CPT1A) (Tables 3 and 4). K-M curves for this signature are shown in Figures 6 to 13.

Importantly, this Mito-Signature yielded a significantly improved hazard-ratio for tumor recurrence of 5.52 (p = 7.3e-10). It was also highly predictive for distant metastasis, in the same group of patients (HR = 5.51; p = 8.1e-07). (See Figures 6). Similar results were obtained in Luminal A LN-negative patients and Luminal B patients (Figure 7).

We also examined the prognostic value of this mitochondrial gene signature in a larger group of ER(+) patients (N = 855), that received hormonal therapy, but not chemotherapy. This group of patients was not segregated into luminal A and luminal B subtypes. Figure 8 shows the results of this K-M analysis for relapse-free survival (HR = 2.80; p = 8.7e-15). Similar results were also obtained distant metastasis-free survival (HR = 2.26; p = 3e-05; N = 548 patients). This mitochondrial signature was also effective if the ER(+) patient population was divided into LN(+) and LN(-) groups (Figure 9).

Next, we assessed the behavior of this Mito-Signature in predicting overall survival. Figure 10 shows that it was also highly predictive of overall survival during hormonal therapy (HR = 3.06; p = 7.8e-05; N = 170 patients).

Moreover, Figure 11 shows that this Mito-Signature was also effective in all ER(+) breast cancer patients in predicting tumor recurrence (N = 3,082), as well as distant metastasis (N = 1,395). Similar results were obtained using data from all breast cancer patients, for recurrence (N = 3,951) and metastasis (N =1,746), as well as for post-progression survival (Figures 12 and 13). Thus, this mitochondrial-based gene signature may represent an important new prognostic tool for predicting patient outcomes, in a wide variety of different breast cancer patients, but especially in ER(+) patients treated with hormonal therapies.

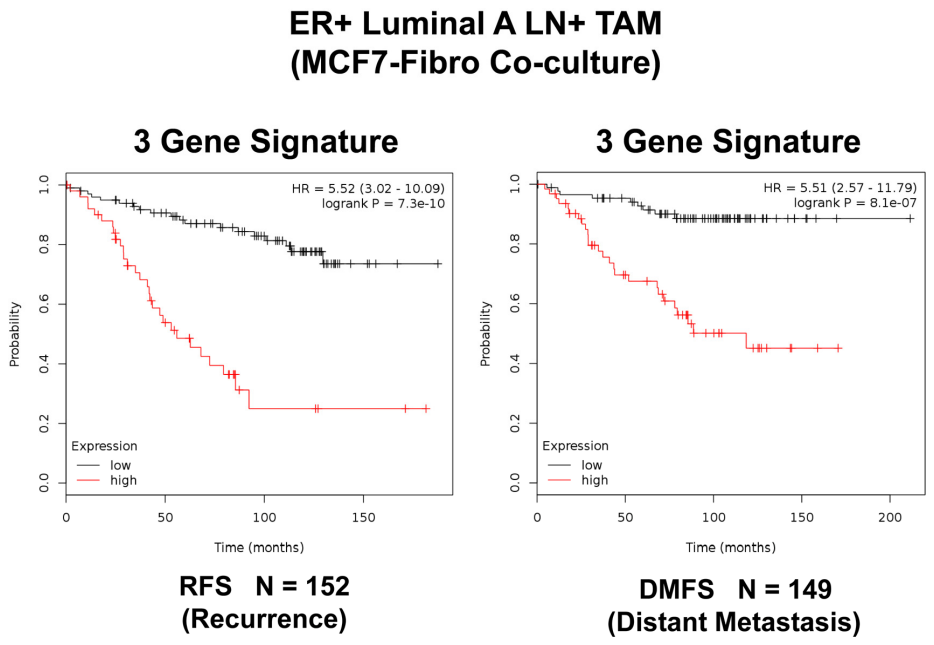

Figure 6. A three-gene based mitochondrial signature (Mito-Signature) that effectively predicts recurrence and distant metastasis in high-risk ER(+) breast cancer patients. Note that this Mito-Signature (HSPD1/VDAC2/CPT1A) predicts tumor recurrence (Left; N = 152 patients; p = 7.3e-10) and distant metastasis (Right; N = 149 patients; p = 8.1e-07) in LN(+) luminal A patients treated with Tamoxifen therapy, indicative of treatment failure and Tamoxifen-resistance. Patients with high-expression levels of the Mito-Signature showed a >5-fold increase in recurrence and distant metastasis, while being treated with hormonal therapy. See also Tables 3 and 4**.** RFS, reccurence-free survival; DMFS, distant metastasis-free survival.

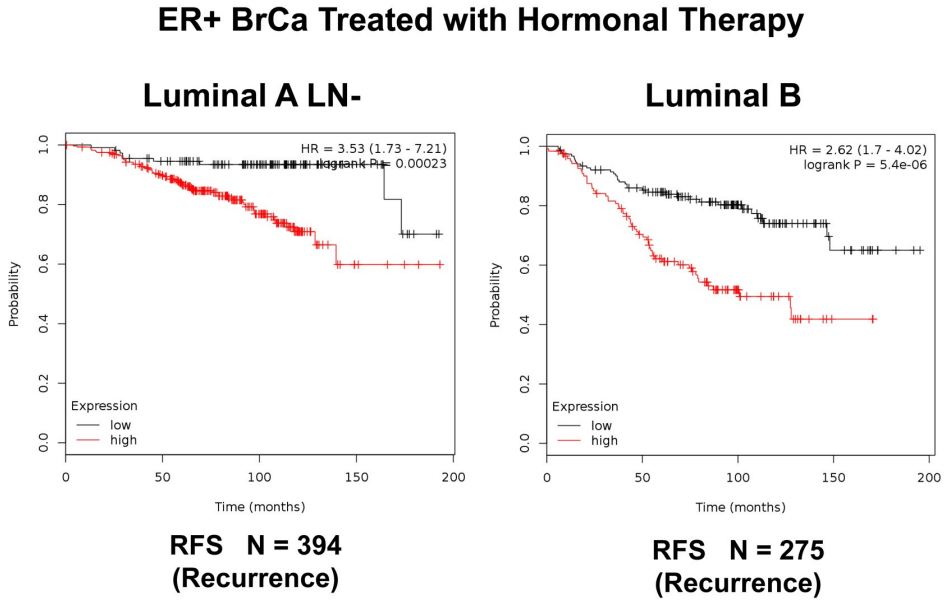

Figure 7. K-M analysis of a Mito-Signature that shows predictive value in Luminal A (LN-negative) and Luminal B breast cancer patients, who were treated with hormonal therapy. Left, Luminal A/LN-negative (N = 394 patients; p =0.00023). Right, Luminal B (N = 275 patients; p = 5.4e-06). Patients with high-expression levels of the Mito- Signature showed a clear increase in recurrence, while being treated with hormonal therapy. RFS, recurrence-free survival.

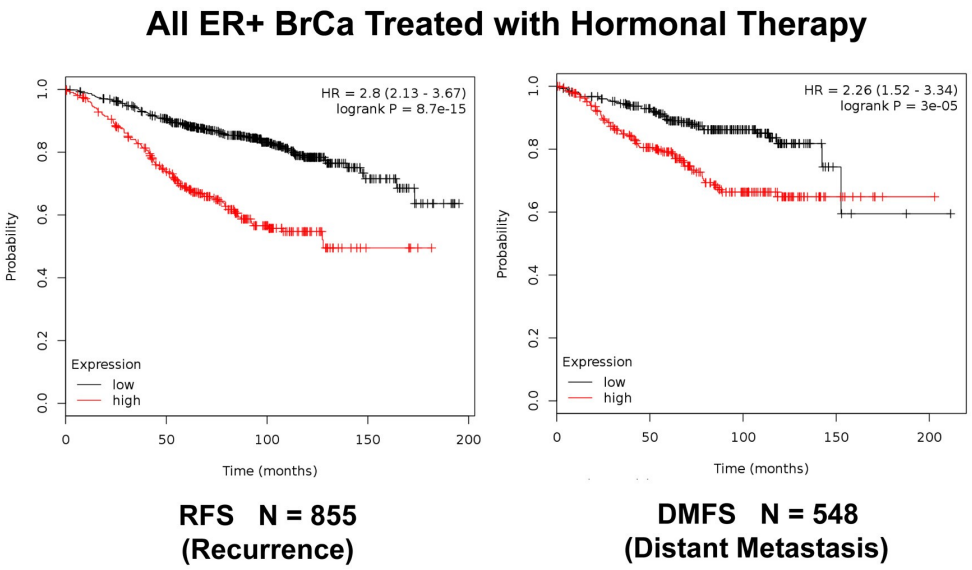

Figure 8. K-M analysis of recurrence and metastasis using a Mito-Signature in a larger group of ER(+) breast cancer patients, who were treated with hormonal therapy. These patients were not sub-divided into luminal A/B subgroups and were not sub-divided by lymph-node status. Note that this Mito-Signature effectively predicts tumor recurrence (Left; N = 855 patients) and distant metastasis (Right; N = 548 patients). Patients with high- expression levels of the Mito-Signature showed a near 3-fold increase in recurrence (p = 8.7e-15) and a >2-fold increase in distant metastasis (p = 3e-05), while being treated with hormonal therapy.

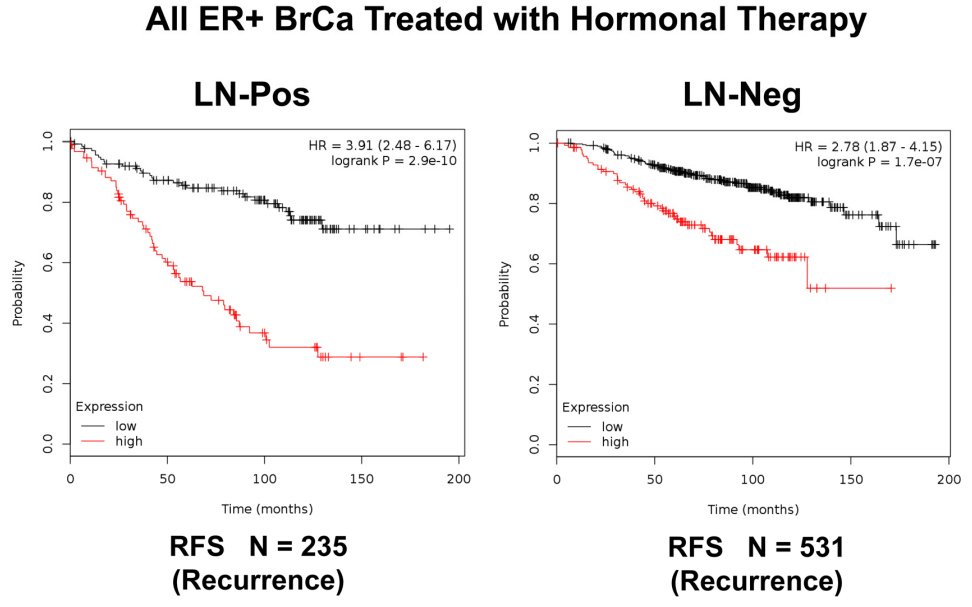

Figure 9. K-M analysis of recurrence using a Mito-Signature in a larger group of ER(+) breast cancer patients, that were divided into sub-groups by lymph node status, who were treated with hormonal therapy. These patients were not sub-divided into luminal A/B subgroups. Left, LN-positive (N = 235 patients). Right, LN-negative (N = 531 patients). Note that LN-positive patients with high-expression levels of the Mito-Signature showed a near 4-fold increase in recurrence, while being treated with hormonal therapy (p = 2.9 e-10). Similar results were observed in LN-negative patients, with a near 3-fold increase in recurrence (p = 1.7e-07). RFS, reccurence-free survival.

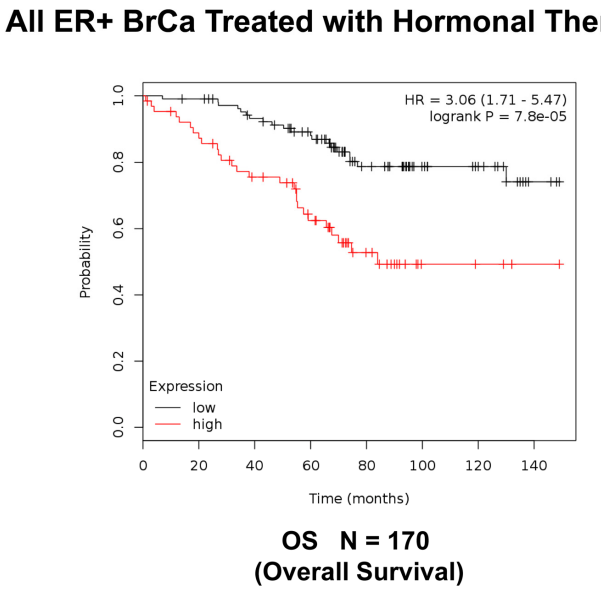

Figure 10. K-M analysis of survival using a Mito-Signature in a group of ER(+) breast cancer. These patients were treated with hormonal therapy. Note that patients with high-expression levels of the Mito- Signature showed a >3-fold reduction in long-term survival (N = 170 patients; p = 7.8e-05). OS, overall survival.

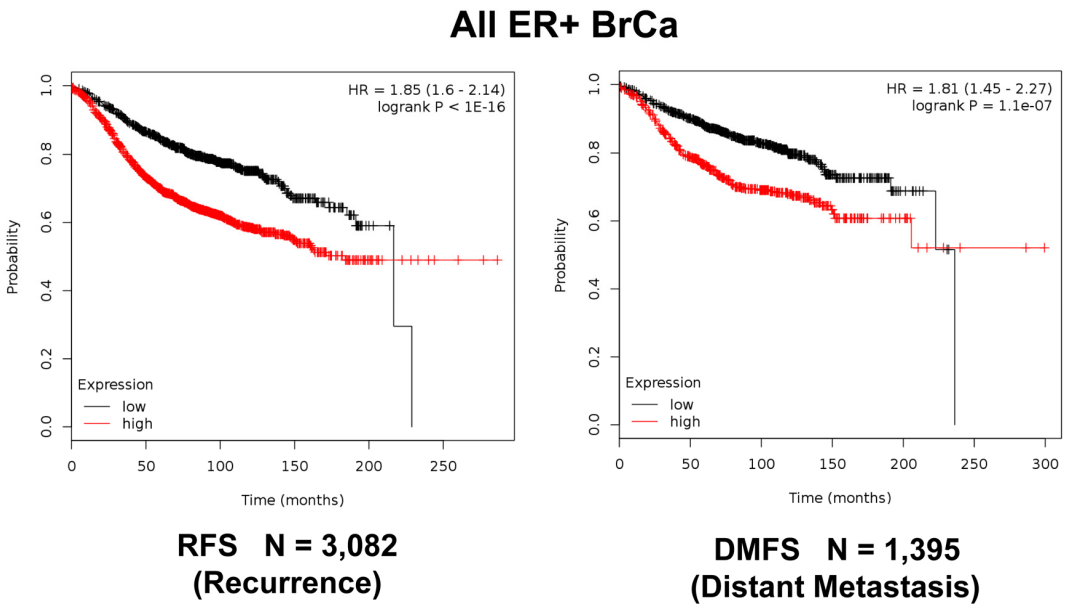

Figure 11. K-M analysis of recurrence and metastasis using a Mito-Signature in a larger group of all ER(+) breast cancer patients, independently of treatment. Patients with high-expression levels of the Mito-Signature showed near 2-fold increases in recurrence (N = 3,082; p < 1e-16) and distant metastasis (N = 1,395; p = 1.1e-07).

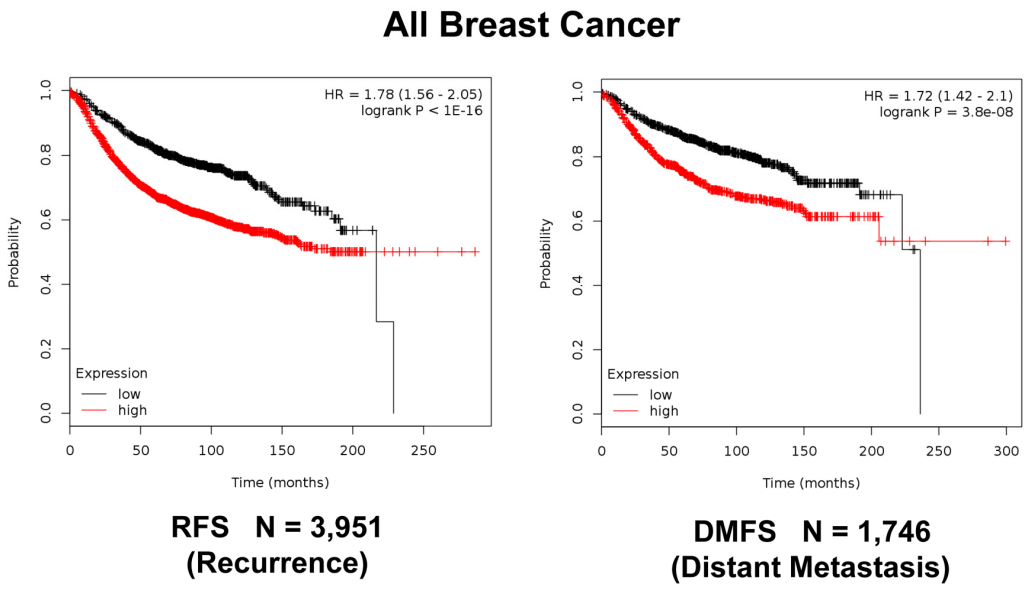

Figure 12. K-M analysis of recurrence and metastasis using a Mito-Signature in a larger group of all breast cancer patients, independently of treatment. Patients with high-expression levels of the Mito-Signature showed near 2-fold increases in recurrence (N = 3,951; p < 1e-16) and distant metastasis (N = 1,746; p = 3.8e-08).

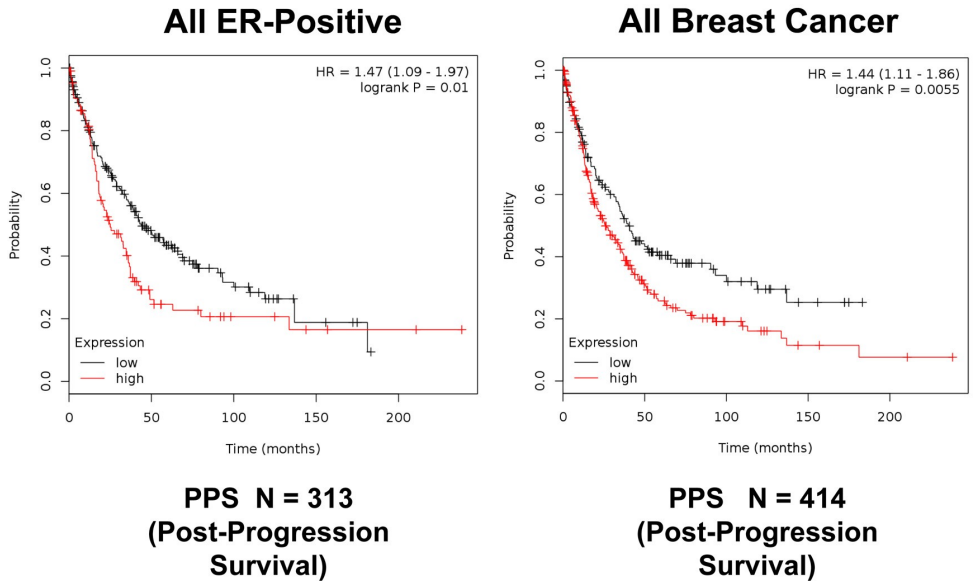

Figure 13. K-M analysis of post-progression survival (PPS) using a Mito-Signature in ER(+) and all breast cancer patients, independently of treatment. Patients with high-expression levels of the Mito-Signature showed near 1.5-fold reductions in post-progression survival. Left, ER(+) (N = 313 patients; p = 0.01). Right, all breast cancer (N = 414 patients; p = 0.0055).

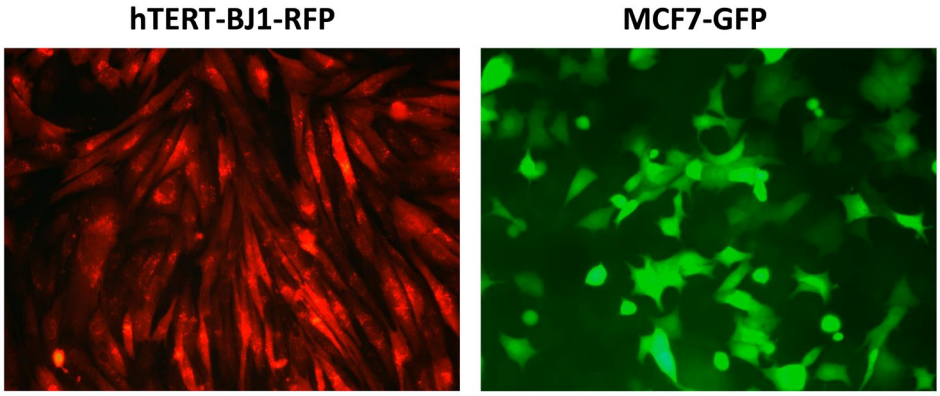

Figure 14. Representative images of hTERT-fibroblasts and MCF7 cells expressing fluorescent proteins. hTERT-BJ1-fibroblasts expressing RFP and MCF7 cells expressing GFP were generated by lentiviral transduction. RFP, red fluorescent protein; GFP, green fluorescent protein.

Markers of fibrosis and glycolysis are up-regulated in MCF7-fibroblast co-cultures, consistent with the onset of oxidative stress

During the co-culture of fibroblasts with cancer cells, it has been observed that their phenotype is drastically changed [17,18]. These changes are related to the induction of various biological processes related oxidative stress, and are consistent with a more myo-fibroblastic phenotype [17,18]. These phenotypic changes include increased expression of cytoskeletal elements and glycolytic enzymes, as well as the elevation of markers of autophagy and senescence [18,21,22]. Therefore, we examined our proteomics data for evidence of these biological processes.

Supplementary Table 10 illustrates that during MCF7-fibroblast co-cultures, many known markers of fibrosis and oxidative stress are actually increased. These changes include the up-regulation of 32 cytoskeletal and extracellular matrix proteins, 11 glycolytic enzymes, 4 lysosomal/autophagy markers and 2 markers of the senescence-associated secretory phenotype, known as SASP.

These findings are also consistent with our results from IPA analysis, shown in Figure 4. Therefore, our results potentially provide interesting new stromal targets for further validation in future studies.

Validating the relevance of MCF7-fibroblast co-cultures for drug development, using FDA-approved antibiotics that target mitochondria

Based on our current findings, we observed that 45 mitochondrial proteins were significantly increased during the co-culture of stromal fibroblasts, with MCF7 cancer cells (Supplementary Table 1). This is consistent with our previous studies employing the vital fluorescent dye MitoTracker, showing that mitochondrial mass is dramatically increased during MCF7-fibroblasts co-cultures [21,22]. This may also have implications for drug sensitivity to mitochondrial inhibitors, especially those targeting mitochondrial biogenesis.

To directly test this hypothesis, we developed an assay system to monitor the sensitivity of cancer cells to drug treatment, in the presence or absence of fibroblasts. For this purpose, we generated hTERT-BJ1-fibroblasts expressing RFP (red fluorescent protein) and MCF7 cells expressing GFP (green fluorescent protein). Representative images of these mono-cultures are shown in Figure 14.

As positive controls for this assay system, we employed two FDA-approved antibiotics (Doxycycline and Azithromycin), which have been shown to act as inhibitors of mitochondrial biogenesis, because of the long-standing evolutionary relationship between mitochondria and bacteria [8,9]. Doxycycline and Azithromycin both inhibit mitochondrial protein translation, as off-target "side-effects", by preferentially affecting the mitochondrial ribosome.

As predicted, Doxycycline preferentially targeted MCF7-GFP cells, during their co-culture with fibroblasts, as directly compared with MCF-GFP mono-cultures (Figure 15). Quantitation of cellular GFP fluorescence was performed using a plate-reader, at the appropriate wavelength (See Materials and Methods). At 500 μM Doxycycline, MCF7-GFP cells in co-culture were ~5-fold more sensitive, than those in mono-cultures. However, the increased sensitivity of MCF7-GFP cells in co-culture was first observed at 100

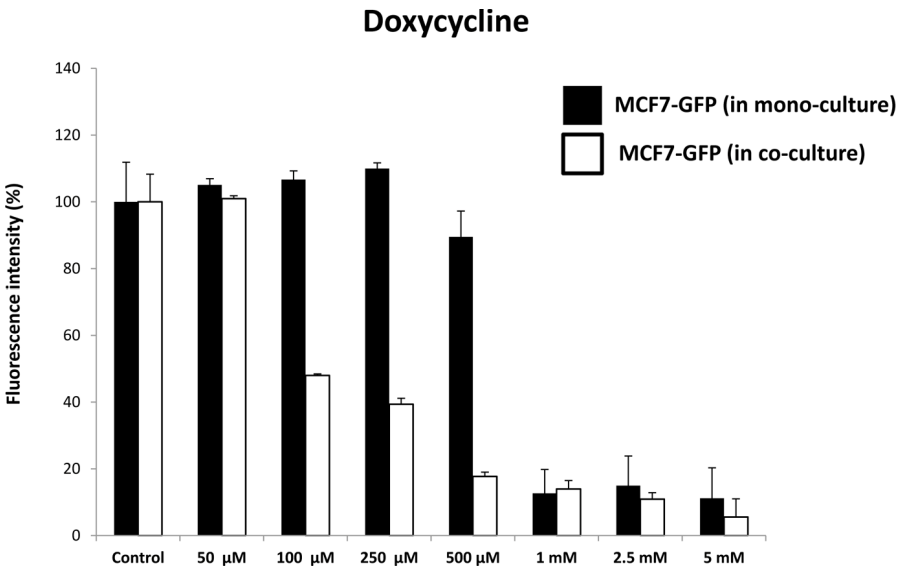

Figure 15. Doxycycline preferentially targets MCF7-GFP cells, during co-culture with fibroblasts: Bar graphs. Note that mono-cultures of MCF7-GFP cells are quantitatively more resistant to the killing effects of Doxycycline, as the concentration of Doxycycline is progressively increased, from 50 µM to 5 mM. Note that at 500 µM Doxycycline, MCF7-GFP cells in co-culture are ~5-fold more sensitive, than those in mono-cultures.

µM, but not at 50 µM. Doxycycline also begins to inhibit overall protein synthesis in mammalian cells, in the range of 100 µM to 1 mM [29]. However, this effect is likely secondary to mitochondrial ATP- depletion (IC-50 = 50 µM) [30]. Therefore, Doxycycline may effectively target both "mito-stemness" and "ribo-stemness" features, by inhibiting both i) mitochondrial protein synthesis and ii) overall protein synthesis.

Representative images of these MCF7-fibroblast co-cultures and their differential sensitivity to Doxycycline are shown in Figure 16. Note the progressive reductions in GFP-fluorescence.

Quantitatively similar results were obtained with Azithromycin, another well-established inhibitor of mitochondrial biogenesis (Figure 17). Azithromycin

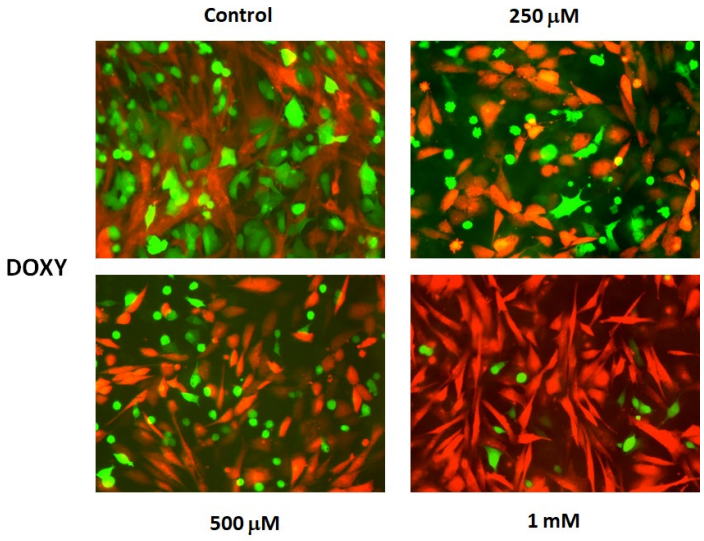

Figure 16. Doxycycline preferentially targets MCF7-GFP cells, during co-culture with fibroblasts: Fluorescence micrographs. Note that as the concentration of Doxycycline is progressively increased, from 250 µM to 1 mM, the green fluorescent signal is decreased.

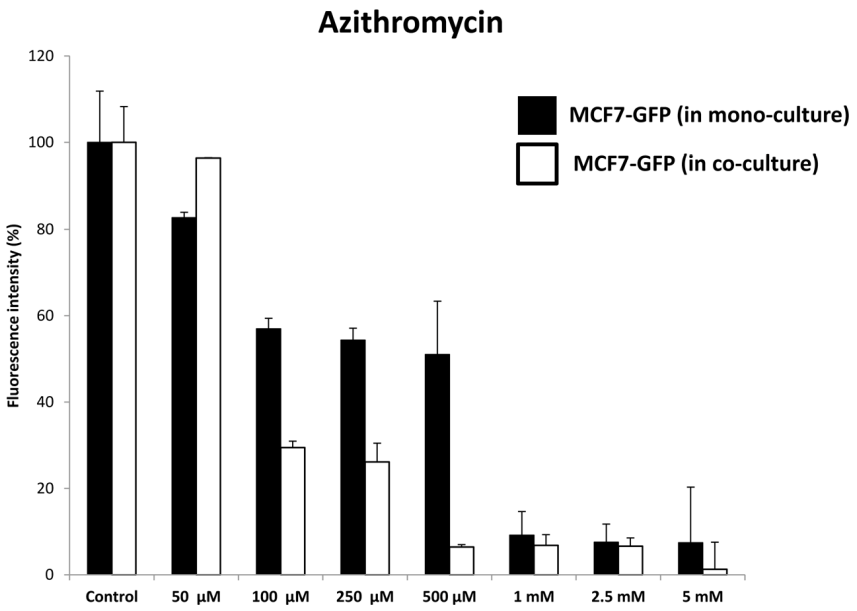

Figure 17. Azithromycin preferentially targets MCF7-GFP cells, during co-culture with fibroblasts: Bar graphs. Note that mono-cultures of MCF7-GFP cells are quantitatively more resistant to the killing effects of Azithromycin, as the concentration of Azithromycin is progressively increased, from 50 µM to 5 mM. Note that at 500 µM Azithromycin, MCF7-GFP cells in co-culture are ~8-fold more sensitive, than those in mono-cultures.

preferentially targeted MCF7-GFP cells, in co-culture with fibroblasts. At 500 µM Azithromycin, MCF7-GFP cells in co-culture were ~8-fold more sensitive, than those in mono-cultures.

These pharmacological data (representing enhanced sensitivity to mitochondrial protein translation inhibitors) are consistent with the increases in mitochondrial biogenesis that we observed by proteomics analysis in MCF7-fibroblast co-cultures.

DISCUSSION

Here, we have used MCF7-fibroblast co-cultures as a model system to dissect the molecular basis of Tamoxifen-resistance. Previously, we showed that MCF7-fibroblasts co-cultures are protected against apoptosis induced by hormonal therapies, such as Tamoxifen and Fulvestrant [16], and that this resistance could be reversed by using Metformin, a known mitochondrial inhibitor [16]. Metformin acts as an OXPHOS inhibitor and activates AMP-kinase, by functionally inactivating mitochondrial Complex I activity. However, the molecular targets that confer resistance to hormonal therapy in this epithelial-stromal model have remained elusive, although it was noted that mitochondrial mass was increased in MCF7 cells, as seen by vital staining with the probe MitoTracker [21,22].

To identify potential new therapeutic targets, we subjected this co-culture system to unbiased label-free proteomics analysis. Using this approach, we observed the induction of both "mito-stemness" and "ribo-stemness" features, consistent with the induction of a more stem-like phenotype (Figure 18). In further support of this notion, the epithelial CSC marker KRT19 was induced nearly 6-fold. KRT19 is currently used clinically to identify metastatic breast cancer cells in sentinel lymph-node biopsies [24,25].

The specific candidate targets identified by proteomics analysis were then intersected with a wealth of publically-available clinical data, first to validate their expression in human breast cancer cells *in vivo*. These clinical samples were subjected to laser-capture micro-dissection to separate human breast cancer cells, from adjacent tumor stroma, before they were subjected to mRNA-based transcriptional profiling.

Unfortunately, we cannot rule out that some of the protein products that we observed were up-regulated in the MCF7-fibroblast co-cultures, were simply due to cancer cell proliferation. Nevertheless, these candidates were further intersected with transcriptional profiling data derived from human breast cancer samples, providing independent cell-type specific validation for their clinical relevance. Therefore, this approach provides an effective workflow to generate new

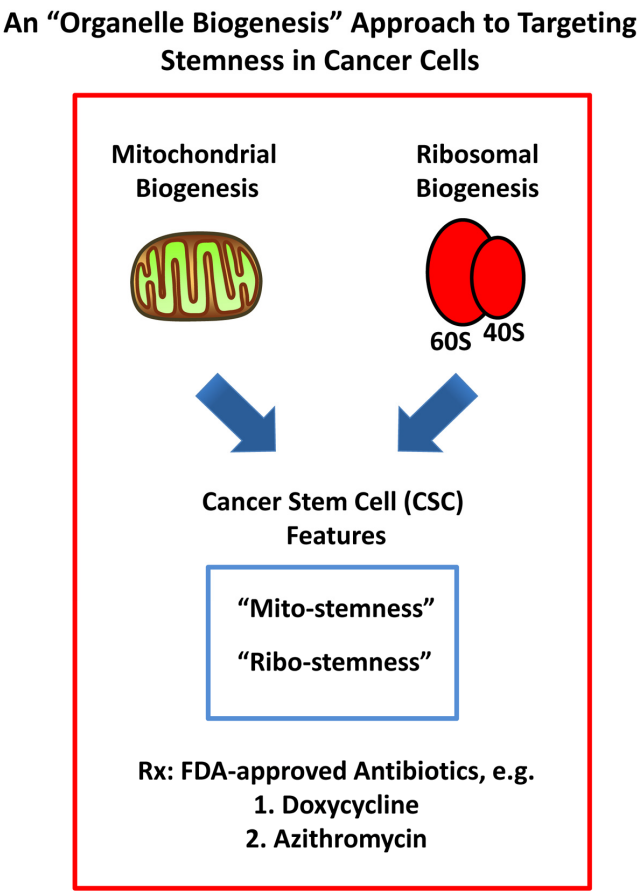

Figure 18. An "organelle biogenesis" approach to cancer therapy. A schematic diagram illustrating that breast cancer cells in co-culture increase their "mito-stemness" and "ribo-stemness" features is shown. Note the increases in mitochondrial biogenesis and the protein synthesis machinery, as enumerated in Supplementary Tables 1 to 4 and independently confirmed by Ingenuity Pathway Analysis (IPA). These findings predict increased susceptibility to treatment with FDA-approved antibiotics, such as Doxycycline and Azithromycin.

candidate targets and a means for their clinical validation.

To assess whether these candidate biomarkers could be used as companion diagnostics for Tamoxifen-resistance, we used the targets identified by proteomics to construct a mitochondrial gene signature. Then, using publically-available clinical outcome data, we stringently evaluated the prognostic value of this Mito-Signature, which effectively predicted tumor recurrence and distant metastasis in breast cancer patients that were treated with Tamoxifen or hormonal therapy. The development of recurrence or metastasis during Tamoxifen treatment is a clear sign of treatment failure and is an accepted clinical hallmark of Tamoxifen-resistance.

We next assessed a possible treatment strategy to selectively sensitize MCF7 cells in co-culture, based on their apparent increase in mitochondrial biogenesis. For this purpose, we devised a co-culture system employing fluorescently-labeled MCF7 cells and fibroblasts. In this system, MCF7 cells expressing GFP were co- cultured with hTERT-BJ1 fibroblasts expressing RFP, so that these two cellular components were easily distinguishable.

We hypothesized that certain FDA-approved antibiotics that target host protein synthesis and mitochondrial protein translation as off-target side effects might be able to sensitize MCF7 cells, under co-culture conditions. Interestingly, our results indicate that MCF7 cells in co-culture were ~5-fold more sensitive to the effects of Doxycycline and ~8-fold more sensitive to the effects of Azithromycin. Therefore, the targeting of mitochondrial protein translation via drug repurposing may be an effective anti-cancer strategy, especially under these more physiologically-relevant culture

conditions, which includes a stromal tumor-micro-environment.

Other recent studies using mono-cultures of MCF7 cells have also suggested a role for increased mitochondrial OXPHOS, in conferring Tamoxifen-resistance. For example, Tamoxifen-resistant MCF7 cells, derived from long-term cell culture with increasing concentrations of Tamoxifen, showed an increase in mitochondrial mass and mitochondrial-dependent ATP production [31]. Similarly, over-expression of a somatic mutation of the estrogen receptor (ESR1-Y537S) normally associated with the clinical development of Tamoxifen-resistance in patients, also increased mitochondrial mass and mitochondrial-dependent ATP production [32]. Therefore, three independent models of Tamoxifen-resistance mechanistically appear to show the same or a very similar mitochondrial phenotype.

As such, this highly-suggestive data implies that mitochondrial inhibitors should be tested clinically as a possible therapeutic option for the prevention and/or treatment of Tamoxifen-resistance or perhaps other forms of hormonal therapy resistance.

In this context, it is interesting to note that one of the recognized off-target side effects of Tamoxifen is that it behaves as a *bonafide* inhibitor of mitochondrial complex III and complex IV [33], while simultaneously inducing oxidative stress. Therefore, Tamoxifen treatment itself may lead to drug resistance, simply by stimulating mitochondrial biogenesis in response to its own intrinsic anti-mitochondrial activity, rather than via its direct or targeted effects on ER-alpha signaling. It is interesting to also consider these anti-mitochondrial effects of Tamoxifen, given the proposed metabolic etiology of breast cancer pathogenesis, related to mitochondrial biogenesis [34,35].

In summary, we conclude that the observed increases in "organelle biogenesis" (i.e., mitochondria and ribosomes) may represent new metabolic hallmarks of a more aggressive cancer cell phenotype. We propose that these findings can be exploited to design more broadly-applicable therapeutics and predictive companion diagnostics, to target stemness features in multiple cancer types. Our results highlight the potential clinical utility of this "organelle biogenesis" approach to cancer therapy (Figure 18).

MATERIALS AND METHODS

Cell culture

Cell culture experiments were carried out using human skin fibroblasts immortalized with the human telomerase reverse transcriptase (hTERT-BJ1 cells) and human MCF7 breast cancer cells. hTERT-BJ1 fibroblasts and MCF7 cells were maintained in complete media: DMEM (D6546, Sigma) supplemented with 10% fetal bovine serum (F7524, Sigma), 100 units/ml of penicillin, 100 µg/ml, streptomycin (P0781, Sigma) and 1% Glutamax (#35050087, Life Technologies). For all experiments, cells were incubated at 37°C in a humidified atmosphere containing 5% CO2.

Co-culture versus mixed cell populations

MCF7 cells and fibroblasts were co-cultured in the presence of Nu-Serum, essentially as we previously described [16-18]. Two million MCF7 cells were co-cultured in a regular 15 cm dish with two million hTERT-BJ1 fibroblasts, seeded in a 1:1 ratio. Likewise, the same numbers of either MCF7 cells or hTERT-BJ1 fibroblasts were seeded separately in 15 cm dishes as monocultures. After 72h of cell culture cells were lysed in RIPA lysis buffer (R0278, Sigma) containing proteinase inhibitors (05 892 970 001, Roche) and kept at 4° C for 20 minutes with rotation. Lysates were cleared by centrifugation for 10 minutes at 10,000 x g and supernatants were collected. The protein concentration of the lysates was determined by using the BCA protein assay kit (23225, Pierce). Briefly, four µg of MCF7- hTERT-BJ1 co-culture lysate or two µg of hTERT-BJ1 monoculture lysate mixed with 2 µg of MCF7 monoculture protein lysate (4 µg of protein in total) were submitted to the CRUK Proteomics Core Facility, for label-free proteomic analysis. Proteomics and statistical analyses were carried out on a fee-for-service basis by Dr. Duncan Smith and his colleagues, at the Proteomics Core Facility at the Cancer Research UK Manchester Institute, University of Manchester.

Label-free proteomics analysis

Chemicals and sample preparation

Formic acid, trifluoroacetic acid, ammonium formate (10 M), ammonium bicarbonate TCEP (Tris (2-carboxyethyl)phosphine hydrochloride), MMTS (Methyl methanethiosulfonate) and trypsin were all obtained from Sigma. HPLC gradient grade acetonitrile was obtained from Fisher Scientific.

Protein digestion

Lysate samples were thawed to room temperature and their concentrations equalised to 1 µg/µL (50 µL volume) with RIPA buffer, and further processed for trypsin digestion by sequential reduction of disulphide bonds with TCEP and alkylation with MMTS. Briefly, 1 µL benzonase (Novagen) was added to the 50 µL aliquot and placed on ice for 15 minutes. The sample

was then taken to dryness using a SpeedVac, and resuspended in 22.5 µL trypsin reaction buffer (40 mM ammonium bicarbonate and 9% acetonitrile). One µL of 50 mM TCEP solution was added to each sample, mixed briefly and placed on a heater block at 60°C for 60 minutes. After cooling to room temperature, 0.5 µL of 200 mM MMTS solution was added to each sample and allowed to react for 15 minutes. Trypsin was added in two waves to ensure efficient digestion of the sample. Firstly, 20 µg of sequencing grade trypsin was resuspended in 1800 µL of trypsin reaction buffer; 225 µL of this solution were added to each sample for digestion, and the reactions were left at 37°C overnight with shaking (600 rpm). The following morning, a further aliquot of trypsin was added. Two ml of trypsin reaction buffer was added to 20 µL of sequencing grade trypsin; 250 µL of this solution were added to each of the digest samples from overnight, and the reactions were left at 37°C for 4 hours with shaking (600 rpm). Thirty-five µL 10% formic acid were added to the 500 µL digest sample (0.7% final concentration of formic acid) to stop the digestion. The digested solution was diluted in 7.5 mL of acetonitrile containing 0.3% formic acid.

HILIC solid phase extraction (SPE) of peptides

PolyhydroxyethylA SPE 12 µm, 300A, 300 mg cartridges (obtained from PolyLC) were used for the HILIC procedure. Prior to use, cartridges required an overnight soak in 50 mM formic acid followed by rinsing with water the following day. Cartridges were preconditioned with 2 mL of Buffer A (90% acetonitrile, 5 mM ammonium formate, pH 2.7) followed by 2 mL of Buffer B (5 mM ammonium formate, pH 2.7) and finally re-equilibrated with 10 mL Buffer A. The diluted samples were loaded onto the cartridges and washed with a further 10 mL Buffer A. Finally, peptides were eluted in 1 mL Buffer C (9 parts Buffer B plus 1 part Buffer A) and the samples dried on a Speedvac to remove organic solvent prior to LCMS/MS analysis.

LC-MS/MS analysis

Lyophilized digests were resuspended in 50 µL of 0.1% TFA to give an approximate concentration of 1 µg/µL. One µL injection volumes were used throughout resulting in an on-column peptide loading of approximately 1 µg per injection. Analysis was performed in quintuplicate for each sample type. All LC-MS/MS analyses were performed on an LTQ Orbitrap XL mass spectrometer coupled to an Ultimate 3000 RSLCnano system (Thermo Scientific). One µL injection volumes were used throughout and samples loaded directly onto the analytical column, PepMap RSLC C18, 2 µm × 75 µm id × 50 cm (Thermo Scientific). The composition (v/v) of LC buffers were as follows; Buffer A - 99.9% water plus 0.1% formic acid and Buffer B - 80% acetonitrile, 19.9% water and 0.1% formic acid. Peptides were loaded directly onto the column at a flow rate of 400 nl/min with an initial mobile phase composition of 1% B. The organic strength was increased linearly from 1% to 22.5% B over 22.5 minutes again at 400 nl/min, followed by an increase to 24.8% B over the next 2.6 minutes with a concomitant reduction in flow rate to 300 nl/min, and to 39% B over a further 14 minutes. A further increase to 60% B over the next 5 minutes was followed by a ramp to 95% B over 2.5 minutes where it was held for a further 2 minutes. The column was then allowed to re-equilibrate to 1% B for a total analysis time of 74 minutes. The mass spectrometer was instructed to perform data dependent acquisition on the top six precursor ions, which were measured in the Orbitrap FTMS detector over the mass range 370–1200 m/z, at a nominal resolution of 60,000. MS/MS spectra were acquired in the ion trap under CID conditions with normalized collision energy of 35, isolation width of 3 Th, Q value of 0.25 and 30 ms activation time. Gas-phase fractionation was performed on the five replicate injections such that MS/MS data was collected for precursor ion range 370–494 m/z Injection 1, 494–595 m/z Injection 2, 595–685 m/z Injection 3, 685–817 m/z Injection 4 and 817–1200 m/z Injection 5.

Statistical analysis

Xcalibur raw data files acquired on the LTQ-Orbitrap XL were directly imported into Progenesis LCMS software (Waters Corp) for peak detection and alignment. Data were analysed using the Mascot search engine. Five replicates were analysed for each sample type. Statistical analyses were performed using ANOVA and only fold-changes in proteins with a p-value less than 0.05 were considered significant.

Ingenuity pathway analyses

Pathway and function analyses were generated using Ingenuity Pathway Analysis (IPA) (Ingenuity systems, http://www.ingenuity.com), which assists with proteomics data interpretation via grouping differentially expressed genes or proteins into known functions and pathways. Pathways with a z score > 1.9 were considered as significantly activated, and pathways with a z score < −1.9 were considered as significantly inhibited.

Validation with transcriptional profiling of breast cancer patient samples

To directly establish the clinical relevance of our findings from proteomics analysis of MCF7-fibroblast co-cultures, we re-analyzed the publically-available transcriptional profiles [26] of epithelial breast cancer cells and adjacent tumor stromal cells that were

physically separated by laser-capture microdissection (from N=28 human breast cancer patients).

Validation with Kaplan-Meier (K-M) analyses of breast cancer patient samples

To perform K-M analysis of mitochondrial gene transcripts, we used an open-access online survival analysis tool to interrogate publically available microarray data from up to 3,455 breast cancer patients [27]. This allowed us to determine their prognostic value [28]. For this purpose, we primarily analyzed data from ER(+) patients that were LN(+) at diagnosis and were of the luminal A sub-type, that were primarily treated with Tamoxifen and not other chemotherapy (N=152 patients). In this group, 100% the patients received some form of hormonal therapy and ~95% of them received Tamoxifen. Biased and outlier array data were excluded from the analysis. This allowed us to identify mitochondrial gene transcripts, with significant prognostic value. Hazard-ratios were calculated, at the best auto-selected cut-off, and p- values were calculated using the logrank test and plotted in R. K-M curves were also generated online using the K-M-plotter (as high-resolution TIFF files), using univariate analysis:

http://kmplot.com/analysis/index.php?p=service&cancer=breast

This allowed us to directly perform in silico validation of these mitochondrial biomarker candidates. The multi-gene classifier function of the program was used to test the prognostic value of short mitochondrial gene signatures, using the mean expression of the selected probes.

Validation via drug treatment of fluorescently-labeled MCF7-fibroblast co-cultures

hTERT-BJ1-RFP cells and MCF7-GFP cells were first generated by stable transduction with lenti-viral vectors. Then, these cells were plated into clear flat bottom 96-well black microplates (Corning; CLS3603**).** Mono-cultures were generated by plating either hTERT-BJ1-RFP (8,000 cells/well) or MCF7-GFP cells (8,000 cells/well). In parallel, co-cultures were generated by co-plating hTERT-BJ1-RFP (6,000 cells/well) with MCF7-GFP (2,000 cells/well). The next day, the plates were treated with either Doxycycline or Azithromycin (or vehicle controls) and were incubated for 72 hours at 37ºC. The cell culture plates were then read with a plate-reader at 545/590 nm (for RFP) and at 490/510 nm (for GFP). Background readings were subtracted from the fluorescent signal and data were then normalized to controls.

AUTHOR CONTRIBUTIONS

MPL and FS conceived and initiated this project. Experiments described in this paper were performed by MPP, when she was previously a post-doctoral fellow in the Lisanti/Sotgia laboratory. BO performed the co-culture experiments, revealing increased sensitivity to FDA-approved antibiotics, which inhibit mitochondrial protein translation. MPL performed the biomarker analysis and generated the K-M curves for predicting clinical outcome. MPL and FS wrote the first draft of the manuscript, which was then further edited by MPP and BO.

ACKNOWLEDGEMENTS

We are grateful to Rumana Rafiq, for her kind and dedicated assistance, in keeping the Translational Medicine Laboratory at Salford running very smoothly. We would like to thank the Foxpoint Foundation and the Healthy Life Foundation for their philanthropic donations, towards new equipment and infrastructure, in the Translational Medicine Laboratory at the University of Salford.

CONFLICTS OF INTEREST

MPL and FS hold a minority interest in Lunella Biotech, Inc.

FUNDING

The Sotgia/Lisanti Laboratory at the University of Salford is funded by Lunella Biotech, Inc.

REFERENCES

1. Peiris-Pagès M, Martinez-Outschoorn UE, Pestell RG, Sotgia F, Lisanti MP. Cancer stem cell metabolism. Breast Cancer Res. 2016; 18:55. https://doi.org/10.1186/s13058-016-0712-6 PMID:27220421

2. De Francesco EM, Sotgia F, Lisanti MP. Cancer stem cells (CSCs): metabolic strategies for their identification and eradication. Biochem J. 2018; 475:1611–34. https://doi.org/10.1042/BCJ20170164 PMID:29743249

3. Martinez-Outschoorn UE, Peiris-Pagés M, Pestell RG, Sotgia F, Lisanti MP. Cancer metabolism: a therapeutic perspective. Nat Rev Clin Oncol. 2017; 14:11–31. https://doi.org/10.1038/nrclinonc.2016.60 PMID:27141887

4. Luo M, Wicha MS. Targeting Cancer Stem Cell Redox Metabolism to Enhance Therapy Responses. Semin Radiat Oncol. 2019; 29:42–54. https://doi.org/10.1016/j.semradonc.2018.10.003 PMID:30573183

5. Yu Z, Pestell TG, Lisanti MP, Pestell RG. Cancer stem cells. Int J Biochem Cell Biol. 2012; 44:2144–51. https://doi.org/10.1016/j.biocel.2012.08.022 PMID:22981632

6. Lamb R, Harrison H, Hulit J, Smith DL, Lisanti MP, Sotgia F. Mitochondria as new therapeutic targets for eradicating cancer stem cells: quantitative proteomics and functional validation via MCT1/2 inhibition. Oncotarget. 2014; 5:11029–37. https://doi.org/10.18632/oncotarget.2789 PMID:25415228

7. Lamb R, Harrison H, Smith DL, Townsend PA, Jackson T, Ozsvari B, Martinez-Outschoorn UE, Pestell RG, Howell A, Lisanti MP, Sotgia F. Targeting tumor-initiating cells: eliminating anabolic cancer stem cells with inhibitors of protein synthesis or by mimicking caloric restriction. Oncotarget. 2015; 6:4585–601. https://doi.org/10.18632/oncotarget.3278 PMID:25671304

8. Lamb R, Ozsvari B, Lisanti CL, Tanowitz HB, Howell A, Martinez-Outschoorn UE, Sotgia F, Lisanti MP. Antibiotics that target mitochondria effectively eradicate cancer stem cells, across multiple tumor types: treating cancer like an infectious disease. Oncotarget. 2015; 6:4569–84. https://doi.org/10.18632/oncotarget.3174 PMID:25625193

9. Ozsvari B, Fiorillo M, Bonuccelli G, Cappello AR, Frattaruolo L, Sotgia F, Trowbridge R, Foster R, Lisanti MP. Mitoriboscins: mitochondrial-based therapeutics targeting cancer stem cells (CSCs), bacteria and pathogenic yeast. Oncotarget. 2017; 8:67457–72. https://doi.org/10.18632/oncotarget.19084 PMID:28978045

10. Ozsvari B, Sotgia F, Simmons K, Trowbridge R, Foster R, Lisanti MP. Mitoketoscins: novel mitochondrial inhibitors for targeting ketone metabolism in cancer stem cells (CSCs). Oncotarget. 2017; 8:78340–50. https://doi.org/10.18632/oncotarget.21259 PMID:29108233

11. Ozsvari B, Bonuccelli G, Sanchez-Alvarez R, Foster R, Sotgia F, Lisanti MP. Targeting flavin-containing enzymes eliminates cancer stem cells (CSCs), by inhibiting mitochondrial respiration: vitamin B2 (Riboflavin) in cancer therapy. Aging (Albany NY). 2017; 9:2610–28. https://doi.org/10.18632/aging.101351 PMID:29253841

12. Ozsvari B, Sotgia F, Lisanti MP. Exploiting mitochondrial targeting signal(s), TPP and bis-TPP, for eradicating cancer stem cells (CSCs). Aging (Albany NY). 2018; 10:229–40. https://doi.org/10.18632/aging.101384 PMID:29466249

13. Sotgia F, Ozsvari B, Fiorillo M, De Francesco EM, Bonuccelli G, Lisanti MP. A mitochondrial based oncology platform for targeting cancer stem cells (CSCs): MITO-ONC-RX. Cell Cycle. 2018; 17:2091–100. https://doi.org/10.1080/15384101.2018.1515551 PMID:30257595

14. Fiorillo M, Sotgia F, Lisanti MP. "Energetic" Cancer Stem Cells (e-CSCs): A New Hyper-Metabolic and Proliferative Tumor Cell Phenotype, Driven by Mitochondrial Energy. Front Oncol. 2019; 8:677. https://doi.org/10.3389/fonc.2018.00677 PMID:30805301

15. Cuyàs E, Verdura S, Folguera-Blasco N, Bastidas-Velez C, Martin ÁG, Alarcón T, Menendez JA. Mitostemness. Cell Cycle. 2018; 17:918–26. https://doi.org/10.1080/15384101.2018.1467679 PMID:29886796

16. Martinez-Outschoorn UE, Goldberg A, Lin Z, Ko YH, Flomenberg N, Wang C, Pavlides S, Pestell RG, Howell A, Sotgia F, Lisanti MP. Anti-estrogen resistance in breast cancer is induced by the tumor microenvironment and can be overcome by inhibiting mitochondrial function in epithelial cancer cells. Cancer Biol Ther. 2011; 12:924–38. https://doi.org/10.4161/cbt.12.10.17780 PMID:22041887

17. Pavlides S, Whitaker-Menezes D, Castello-Cros R, Flomenberg N, Witkiewicz AK, Frank PG, Casimiro MC, Wang C, Fortina P, Addya S, Pestell RG, Martinez-Outschoorn UE, Sotgia F, Lisanti MP. The reverse Warburg effect: aerobic glycolysis in cancer associated fibroblasts and the tumor stroma. Cell Cycle. 2009; 8:3984–4001. https://doi.org/10.4161/cc.8.23.10238 PMID:19923890

18. Martinez-Outschoorn UE, Lisanti MP, Sotgia F. Catabolic cancer-associated fibroblasts transfer energy and biomass to anabolic cancer cells, fueling tumor growth. Semin Cancer Biol. 2014; 25:47–60. https://doi.org/10.1016/j.semcancer.2014.01.005 PMID:24486645

19. Peiris-Pagès M, Sotgia F, Lisanti MP. Chemotherapy induces the cancer-associated fibroblast phenotype,

activating paracrine Hedgehog-GLI signalling in breast cancer cells. Oncotarget. 2015; 6:10728–45. https://doi.org/10.18632/oncotarget.3828 PMID:25915429

20. Peiris-Pagès M, Smith DL, Győrffy B, Sotgia F, Lisanti MP. Proteomic identification of prognostic tumour biomarkers, using chemotherapy-induced cancer-associated fibroblasts. Aging (Albany NY). 2015; 7:816–38. https://doi.org/10.18632/aging.100808 PMID:26539730

21. Martinez-Outschoorn UE, Lin Z, Trimmer C, Flomenberg N, Wang C, Pavlides S, Pestell RG, Howell A, Sotgia F, Lisanti MP. Cancer cells metabolically "fertilize" the tumor microenvironment with hydrogen peroxide, driving the Warburg effect: implications for PET imaging of human tumors. Cell Cycle. 2011; 10:2504–20. https://doi.org/10.4161/cc.10.15.16585 PMID:21778829

22. Martinez-Outschoorn UE, Balliet RM, Rivadeneira DB, Chiavarina B, Pavlides S, Wang C, Whitaker-Menezes D, Daumer KM, Lin Z, Witkiewicz AK, Flomenberg N, Howell A, Pestell RG, et al. Oxidative stress in cancer associated fibroblasts drives tumor-stroma co-evolution: A new paradigm for understanding tumor metabolism, the field effect and genomic instability in cancer cells. Cell Cycle. 2010; 9:3256–76. https://doi.org/10.4161/cc.9.16.12553 PMID:20814239

23. Tsuneoka M, Teye K, Arima N, Soejima M, Otera H, Ohashi K, Koga Y, Fujita H, Shirouzu K, Kimura H, Koda Y. A novel Myc-target gene, mimitin, that is involved in cell proliferation of esophageal squamous cell carcinoma. J Biol Chem. 2005; 280:19977–85. https://doi.org/10.1074/jbc.M501231200 PMID:15774466

24. Otsubo R, Hirakawa H, Oikawa M, Baba M, Inamasu E, Shibata K, Hatachi T, Matsumoto M, Yano H, Abe K, Taniguchi H, Nakashima M, Nagayasu T. Validation of a Novel Diagnostic Kit Using the Semidry Dot-Blot Method to Detect Metastatic Lymph Nodes in Breast Cancer: Distinguishing Macrometastases From Nonmacrometastases. Clin Breast Cancer. 2018; 18:e345–51. https://doi.org/10.1016/j.clbc.2017.07.009 PMID:28778378

25. Okamoto S, Niikura H, Nakabayashi K, Hiyama K, Matoda M, Takeshima N, Watanabe M, Nagase S, Otsuki T, Yaegashi N. Detection of sentinel lymph node metastases in cervical cancer: assessment of KRT19 mRNA in the one-step nucleic acid amplification (OSNA) method. Gynecol Oncol. 2013; 130:530–36. https://doi.org/10.1016/j.ygyno.2013.06.027 PMID:23811115

26. Casey T, Bond J, Tighe S, Hunter T, Lintault L, Patel O, Eneman J, Crocker A, White J, Tessitore J, Stanley M, Harlow S, Weaver D, et al. Molecular signatures suggest a major role for stromal cells in development of invasive breast cancer. Breast Cancer Res Treat. 2009; 114:47–62. https://doi.org/10.1007/s10549-008-9982-8 PMID:18373191

27. Győrffy B, Lanczky A, Eklund AC, Denkert C, Budczies J, Li Q, Szallasi Z. An online survival analysis tool to rapidly assess the effect of 22,277 genes on breast cancer prognosis using microarray data of 1,809 patients. Breast Cancer Res Treat. 2010; 123:725–31. https://doi.org/10.1007/s10549-009-0674-9 PMID:20020197

28. Sotgia F, Fiorillo M, Lisanti MP. Mitochondrial markers predict recurrence, metastasis and tamoxifen-resistance in breast cancer patients: early detection of treatment failure with companion diagnostics. Oncotarget. 2017; 8:68730–45. https://doi.org/10.18632/oncotarget.19612 PMID:28978152

29. Contreras A, Vazquez D, Carrasco L. Inhibition, by selected antibiotics, of protein synthesis in cells growing in tissue cultures. J Antibiot (Tokyo). 1978; 31:598–602. https://doi.org/10.7164/antibiotics.31.598 PMID:567213

30. Lamb R, Fiorillo M, Chadwick A, Ozsvari B, Reeves KJ, Smith DL, Clarke RB, Howell SJ, Cappello AR, Martinez-Outschoorn UE, Peiris-Pagès M, Sotgia F, Lisanti MP. Doxycycline down-regulates DNA-PK and radiosensitizes tumor initiating cells: implications for more effective radiation therapy. Oncotarget. 2015; 6:14005–25. https://doi.org/10.18632/oncotarget.4159 PMID:26087309

31. Fiorillo M, Sotgia F, Sisci D, Cappello AR, Lisanti MP. Mitochondrial "power" drives tamoxifen resistance: NQO1 and GCLC are new therapeutic targets in breast cancer. Oncotarget. 2017; 8:20309–27. https://doi.org/10.18632/oncotarget.15852 PMID:28411284

32. Fiorillo M, Sanchez-Alvarez R, Sotgia F, Lisanti MP. The ER-alpha mutation Y537S confers Tamoxifen-resistance via enhanced mitochondrial metabolism, glycolysis and Rho-GDI/PTEN signaling: implicating TIGAR in somatic resistance to endocrine therapy. Aging (Albany NY). 2018; 10:4000–23.

https://doi.org/10.18632/aging.101690
PMID:30573703

33. Tuquet C, Dupont J, Mesneau A, Roussaux J. Effects of tamoxifen on the electron transport chain of isolated rat liver mitochondria. Cell Biol Toxicol. 2000; 16:207–19.
https://doi.org/10.1023/A:1007695308257
PMID:11101003

34. Mazzanti CM, Lessi F, Armogida I, Zavaglia K, Franceschi S, Al Hamad M, Roncella M, Ghilli M, Boldrini A, Aretini P, Fanelli G, Marchetti I, Scatena C, et al. Human saliva as route of inter-human infection for mouse mammary tumor virus. Oncotarget. 2015; 6:18355–63.
https://doi.org/10.18632/oncotarget.4567
PMID:26214095

35. Lamb R, Bonuccelli G, Ozsvári B, Peiris-Pagès M, Fiorillo M, Smith DL, Bevilacqua G, Mazzanti CM, McDonnell LA, Naccarato AG, Chiu M, Wynne L, Martinez-Outschoorn UE, et al. Mitochondrial mass, a new metabolic biomarker for stem-like cancer cells: understanding WNT/FGF-driven anabolic signaling. Oncotarget. 2015; 6:30453–71.
https://doi.org/10.18632/oncotarget.5852
PMID:26421711

SUPPLEMENTARY MATERIAL

Supplementary Tables

Supplementary Table 1. Proteomics Analysis: Mitochondrial-Related Proteins Up-regulated in MCF7-Fibroblast Co-Cultures.

Gene Symbol	Description	Fold-Increase	Mito-Complex	MRP/Chaperone
NDUFAF2	Mimitin, c-Myc-induced mitochondrial protein; B17.2L (related to NDUFAF4/**HRPAP20**)	Infinity	I	Chaperone
GPD2	Glycerol-3-phosphate dehydrogenase, mitochondrial (ROS/H2O2 Production)	238.91		
AIFM1	Apoptosis-inducing factor 1, mitochondrial (NADH oxidase activity)	237.74	I, III, IV	Chaperone
PRKDC	DNA-dependent protein kinase catalytic subunit (mitochondrial genome maintenance)	102.78		
DNAJA3	HSP40, DnaJ homolog, subfamily A, member 3, mitochondrial	76.43		Chaperone
MRPL43	Mitochondrial ribosomal protein L43	66.38		MRP
COX4I1	Cytochrome c oxidase subunit 4 isoform 1	56.68	IV	
HSPD1	HSP60, 60 kDa heat shock protein, mitochondrial	29.29		Chaperone
MRRF	Ribosome-recycling factor, mitochondrial	23.53		MRP
SLC25A5	Solute Carrier Family 25 (Mitochondrial Carrier; ADP/ATP Translocator), Member 5	14.49		
VDAC2	Voltage-dependent anion-selective channel protein 2	13.60		
UQCRFS1	RISP, Ubiquinol-cytochrome C reductase iron-sulfur subunit, (Rieske iron-sulfur protein)	13.07	III	
VDAC1	Voltage-dependent anion-selective channel protein 1	10.05		
ECH1	Delta(3,5)-Delta(2,4)-dienoyl-CoA isomerase, mitochondrial	8.51		
MCCC2	Methylcrotonoyl-CoA carboxylase beta chain, mitochondrial	4.52		
MRPS28	MRPS28 protein	3.86		MRP
ATP5A1	ATP synthase subunit alpha, mitochondrial (EC 3.6.3.14)	3.83	V	
SUCLG2	Succinyl-CoA ligase [GDP-forming] subunit beta, mitochondrial	3.58		
ABAT	4-aminobutyrate aminotransferase, mitochondrial	3.44		
IMMT	Mitochondrial inner membrane protein	3.27		
AK4	Adenylate kinase isoenzyme 4, mitochondrial	3.02		
GOT2	Aspartate aminotransferase, mitochondrial	2.87		
HSPA9	heat shock 70kDa protein 9 (mortalin), mitochondrial	2.47		Chaperone
TUFM	Elongation factor Tu, mitochondrial	2.37		
CLUH	Clustered mitochondria protein homolog	2.15		
OAT	Ornithine aminotransferase, mitochondrial	2.14		
IDH1	Isocitrate dehydrogenase [NADP], cytoplasmic	2.10		
SLC25A3	Solute carrier family 25 (mitochondrial carrier; phosphate carrier), member 3	2.09		
NDUFA5	NADH dehydrogenase [ubiquinone] 1 alpha subcomplex subunit 5	2.08	I	
UQCRC2	Cytochrome b-c1 complex subunit 2, mitochondrial	2.07	III	
ETFA	Electron transfer flavoprotein subunit alpha, mitochondrial	2.05		
PPA2	Inorganic pyrophosphatase 2, mitochondrial	2.03		
ECHS1	Enoyl-CoA hydratase, mitochondrial	2.02		
PPT1	Palmitoyl-protein thioesterase 1	1.91		

DLD	Dihydrolipoyl dehydrogenase, mitochondrial	1.89		
CHCHD3	Coiled-coil-helix-coiled-coil-helix domain-containing protein 3, mitochondrial	1.89		
ATP5H	ATP synthase subunit d, mitochondrial	1.88	V	
IARS2	Isoleucine--tRNA ligase, mitochondrial	1.86		
LRPPRC	Leucine-rich PPR-motif containing, mitochondrial	1.85		
PC	Pyruvate carboxylase, mitochondrial	1.79		
HADHA	Trifunctional enzyme subunit alpha, mitochondrial	1.74		
SLC25A13	Calcium-binding mitochondrial carrier protein Aralar2	1.74		
TRAP1	Heat shock protein 75 kDa, mitochondrial	1.72		Chaperone
ACADSB	Short/branched chain specific acyl-CoA dehydrogenase, mitochondrial	1.72		
CPT1A	Carnitine palmitoyltransferase 1A, mitochondrial	1.65		

-Proteins listed above (45 in total) were all upregulated in MCF7-Fibroblast Co-cultures ($p < 0.05$). **MRP**, mitochondrial ribosomal proteins

Supplementary Table 2. Proteomics Analysis: Ribosomal Proteins Up-regulated in MCF7-Fibroblast Co-Cultures.

Gene Symbol	Description	Fold-Increase
RPL4	60S ribosomal protein L4	Infinity
RPL15	60S ribosomal protein L15	2,238.12
RPL19	60S ribosomal protein L19	168.84
RPL36AL	60S ribosomal protein L36a-like	54.47
RPL24	60S ribosomal protein L24	43.56
RPL10	60S ribosomal protein L10	42.78
RPL29	60S ribosomal protein L29	20.53
RPL18A	60S ribosomal protein L18a	17.08
RPL8	60S ribosomal protein L8	5.74
RPL34	60S ribosomal protein L34	5.36
RPL13	60S ribosomal protein L13	5.31
RPL14	60S ribosomal protein L14	3.09
RPL3	60S ribosomal protein L3	3.04
RPL27a	60S ribosomal protein L27a	2.99
RPLP2	60S acidic ribosomal protein P2	2.90
RPL6	60S ribosomal protein L6	2.05
RPL5	60S ribosomal protein L5	2.04
RPL28	60S ribosomal protein L28	2.00
RPS29	40S ribosomal protein S29	Infinity
RPS10	40S ribosomal protein S10	74.47
RPS6	40S ribosomal protein S6	23.37
RPS18	40S ribosomal protein S18	9.20
RPS27A	40S ribosomal protein S27a	5.19
RPS2	40S ribosomal protein S2	2.98
RPS27A	40S ribosomal protein S27a	2.96
RPS3A	40S ribosomal protein S3A	2.39
RPS19	40S ribosomal protein S19	2.05
RPS11	40S ribosomal protein S11	2.00

-Proteins listed above (28 in total) were all upregulated in MCF7-Fibroblast Co-cultures ($p < 0.05$).

Supplementary Table 3. Proteomics Analysis: Other Chaperones Up-regulated in MCF7-Fibroblast Co-Cultures.

Gene Symbol	Description	Fold-Increase
HSP90AB1	Heat Shock Protein 90kDa Alpha (Cytosolic), Class B Member 1	Infinity
HSPA5	78 kDa glucose-regulated protein	82.18
HSP90AA1	Heat Shock Protein 90kDa Alpha (Cytosolic), Class A Member 1	79.52
HSPB1	Heat Shock 27kDa Protein 1	35.73
HSPA8	Heat shock cognate 71 kDa protein	8.42
HSPA4	Heat shock 70 kDa protein	5.38
STIP1	Stress-induced-phosphoprotein 1 (HSP70/HSP90-organizing protein)	2.99
CDC37	HSP90 co-chaperone Cdc37	2.83
HSPA2	Heat shock-related 70 kDa protein 2	2.59
HSPH1	Heat shock protein 105 kDa	2.53

-Proteins listed above (10 in total) were all upregulated in MCF7-Fibroblast Co-cultures ($p < 0.05$).

Supplementary Table 4. Proteomics Analysis: Proteins Involved in mRNA Translation Initiation, Polypeptide Elongation, tRNA Synthesis and Amino Acid Uptake are All Up-regulated in MCF7-Fibroblast Co-Cultures.

Gene Symbol	Description	Fold-Increase
Translation initiation factors (required for mRNA binding to ribosomes)		
EIF2S1	Eukaryotic translation initiation factor 2 subunit 1	291.47
EIF3H	Eukaryotic translation initiation factor 3 subunit H	81.05
EIF4H	Eukaryotic translation initiation factor 4H	31.21
EIF4A1	Eukaryotic translation initiation factor 4A-I	18.85
EIF5	Eukaryotic translation initiation factor 5	8.72
EIF3A	Eukaryotic translation initiation factor 3 subunit A	2.94
EIF2S3L	Putative eukaryotic translation initiation factor 2 subunit 3-like protein	2.86
EIF3E	Eukaryotic translation initiation factor 3 subunit E	2.30
EIF3B	Eukaryotic translation initiation factor 3 subunit B	1.85
Elongation factors (promote delivery of aminoacyl tRNAs to the ribosome)		
EEF2	Elongation factor 2	18.96
EEF1G	Elongation factor 1-gamma	2.45
TUFM	Elongation factor Tu, mitochondrial	2.37
EEF1A2	Elongation factor 1-alpha 2	2.36
EEF1A1	Elongation factor 1-alpha	2.03
EEF1D	Elongation factor 1-delta	1.86
Enzymes for tRNA Synthesis		
QARS	Glutamine--tRNA ligase, cytoplasmic	31.90
DARS	Aspartate--tRNA ligase, cytoplasmic	9.69
MARS	Methionine-tRNA synthetase, cytoplasmic	3.44
RTCB	tRNA-splicing ligase RtcB homolog (C22orf28)	3.25
DTD1	D-tyrosyl-tRNA(Tyr) deacylase 1	3.10
YARS	Tyrosine--tRNA ligase, cytoplasmic	2.38
RARS	Arginine--tRNA ligase, cytoplasmic	2.23
AARS	Alanyl-tRNA synthetase, cytoplasmic	2.23
IARS2	Isoleucine--tRNA ligase, mitochondrial	1.86
AIMP2	Aminoacyl tRNA synthase complex-interacting multifunctional protein 2	1.70
GARS	Glycine--tRNA ligase, cytoplasmic	1.70
EPRS	Bifunctional glutamate/proline--tRNA ligase	1.67
TRMT112	tRNA methyltransferase 112 homolog	1.66
Amino Acid Transporters		
SLC6A19	Neutral amino acid transporter B(0)	4.18
SLC7A5	Solute carrier family 7 (Cationic AA transporter, y+ system), member 5	3.05

-Proteins listed above (30 in total) were all upregulated in MCF7-Fibroblast Co-cultures ($p < 0.05$).

Supplementary Table 5. Proteomics Analysis: Markers of Cell Proliferation and Stemness are Up-regulated in MCF7-Fibroblast Co-Cultures.

Gene Symbol	Description	Fold-Increase	Specificity
MKI67	Antigen KI-67	4,531.38	Expressed in all cycling cells, except for resting cells in the G0-phase; Associated also with ribosomal RNA (rRNA) synthesis and, thus, protein synthesis
KRT19	Keratin, type I cytoskeletal 19	5.94	Marker of CSCs and breast cancer metastasis (sentinel lymph node)
PCNA	Proliferating cell nuclear antigen	3.87	Marker for the G1/S phase of the cell cycle

-Proteins listed above were upregulated in MCF7-Fibroblast Co-cultures ($p < 0.05$).
-In human breast cancer cells *in vivo*, KRT19 was transcriptionally up-regulated by 4.39-fold (p=2.66E-05), relative to the adjacent tumor stroma. Similarly, PCNA levels were up-regulated by 3.58-fold (p=3.64E-04).

Supplementary Table 6. Nuclear Mitochondrial Gene Transcripts Up-regulated in Human Breast Cancers (Cancer Epithelia vs. Tumor Stroma).

Gene Symbol	Fold-Increase	P-Value
UQCRFS1	5.71	2.45E-07
MCCC2	5.48	5.78E-07
ATP5A1	5.01	3.09E-06
UQCRC2	4.84	5.73E-06
IMMT	4.71	8.89E-06
IARS2	4.70	9.15E-06
GOT2	4.58	1.40E-05
LRPPRC	4.34	3.15E-05
ECHS1	4.05	8.22E-05
ATP5H	4.01	9.48E-05
VDAC2	3.99	0.0001
DLD	3.78	0.0002
PPT1	3.76	0.0002
SLC25A3	3.76	0.0002
HSPA9	3.69	0.0002
SLC25A5	3.49	0.0005
HSPD1	3.42	0.0006
COX4I1	3.39	0.0007
TUFM	3.38	0.0007
HADHA	3.27	0.0009
PPA2	3.19	0.001
IDH1	3.18	0.001
OAT	3.17	0.001
SUCLG2	3.03	0.002
DNAJA3	2.92	0.003
NDUFA5	2.75	0.004
CHCHD3	2.74	0.004
SLC25A13	2.69	0.005
VDAC1	2.64	0.005
MRPS28	2.25	0.01
PRKDC	2.14	0.02
ABAT	2.08	0.02
ECH1	1.97	0.03
ETFA	1.75	0.04

-Transcriptional profiling data derived from the analysis of N=28 breast cancer patients are shown, high-lighting the levels of fold-upregulation observed in the epithelial cancer cell compartment (relative to the tumor stroma), and corresponding p-values derived from the analysis of these clinical samples.

-Proteins listed above (34 in total) were all upregulated in MCF7-Fibroblast Co-cultures (Compare with **Supplementary Table 1**) ($p < 0.05$).

Supplementary Table 7. Ribosomal Protein Gene Transcripts Up-regulated in Human Breast Cancers (Cancer Epithelia vs. Tumor Stroma).

Gene Symbol	Fold-Increase	P-Value
RPL24	5.38	8.11E-07
RPL3	5.01	3.14E-06
RPL10	4.91	4.48E-06
RPL15	4.60	1.28E-05
RPL13	4.48	1.98E-05
RPL14	4.45	2.15E-05
RPL6	4.00	9.86E-05
RPL19	3.98	0.0001
RPL8	3.86	0.00015
RPLP2	3.80	0.0002
RPL34	3.63	0.0003
RPL4	3.05	0.002
RPL29	2.94	0.002
RPL27A	2.87	0.003
RPL5	2.74	0.004
RPL28	2.33	0.01
RPL18A	2.28	0.01
RPL36AL	1.70	0.048
RPS18	4.96	3.71E-06
RPS27A	4.63	1.19E-05
RPS3A	4.59	1.35E-05
RPS6	4.47	2.04E-05
RPS10	4.18	5.34E-05
RPS19	4.17	5.49E-05
RPS11	3.58	0.0004
RPS2	3.36	0.0007
RPS29	2.31	0.01

-Transcriptional profiling data derived from the analysis of N=28 breast cancer patients are shown, high-lighting the levels of fold-upregulation observed in the epithelial cancer cell compartment (relative to the tumor stroma), and corresponding p-values derived from the analysis of these clinical samples.

-Proteins listed above (27 in total) were all upregulated in MCF7-Fibroblast Co-cultures (Compare with **Supplementary Table 2**). ($p < 0.05$).

Supplementary Table 8. Other Chaperone Gene Transcripts Up-regulated in Human Breast Cancers (Cancer Epithelia vs. Tumor Stroma).

Gene Symbol	Fold-Increase	P-Value
HSP90AB1	4.93	4.03E-06
HSPA5	3.89	0.0001
HSP90AA1	3.76	0.0002
HSPA4	3.75	0.0002
HSPB1	3.27	0.001
HSPH1	3.18	0.001
HSPA8	3.11	0.002

-Transcriptional profiling data derived from the analysis of N=28 breast cancer patients are shown, high-lighting the levels of fold-upregulation observed in the epithelial cancer cell compartment (relative to the tumor stroma), and corresponding p-values derived from the analysis of these clinical samples.

-Proteins listed above (7 in total) were all upregulated in MCF7-Fibroblast Co-cultures (Compare with **Supplementary Table 3**). ($p < 0.05$).

Supplementary Table 9. Transcripts of Genes Associated with mRNA Translation Initiation, Polypeptide Elongation, and tRNA Synthesis Are All Up-regulated in Human Breast Cancers (Cancer Epithelia vs. Tumor Stroma).

Gene Symbol	Fold-Increase	P-Value
Translation initiation factors (required for mRNA binding to ribosomes)		
EIF4H	4.77	7.20E-06
EIF3H	4.70	9.25E-06
EIF5	3.90	0.0001
EIF3E	3.57	0.0004
EIF3A	2.51	0.008
EIF3B	2.21	0.02
Elongation factors (promote delivery of aminoacyl tRNAs to the ribosome)		
EEF2	4.01	9.29E-05
EEF1G	3.71	0.0002
TUFM	3.38	0.0007
EEF1A1	3.16	0.001
EEF1D	2.50	0.008
Enzymes for tRNA Synthesis		
IARS2	4.70	9.15E-06
RTCB	4.59	1.37E-05
MARS	4.35	3.00E-05
EPRS	4.06	8.10E-05
QARS	3.73	0.0002
DARS	3.43	0.0006
DTD1	1.78	0.04
YARS	1.72	0.046

-Transcriptional profiling data derived from the analysis of N=28 breast cancer patients are shown, high-lighting the levels of fold-upregulation observed in the epithelial cancer cell compartment (relative to the tumor stroma), and corresponding p-values derived from the analysis of these clinical samples.
-Proteins listed above (19 in total) were all upregulated in MCF7-Fibroblast Co-cultures (**Compare with Supplemental Table 4**). ($p < 0.05$).

Supplementary Table 10. Proteomics Analysis: Stromal CAF Markers are Up-regulated in MCF7-Fibroblast Co-Cultures

Gene Symbol	Description	Fold-Increase
Glycolytic Enzymes		
PKM	Pyruvate kinase	Infinity
LDHA	L-Lactate dehydrogenase A	426.16
PGD	6-Phosphogluconate dehydrogenase, decarboxylating	13.59
ENO1	Alpha-Enolase	11.60
ALDOA	Fructose-bisphosphate aldolase	7.14
PGI	Glucose-6-phosphate isomerase	5.02
PFK	6-Phosphofructokinase	4.14
PGK1	Phosphoglycerate kinase 1	4.38
TPI1	Triosephosphate isomerase 1	2.66
G6PD	Glucose-6-phosphate 1-dehydrogenase	2.28
Cytoskeletal and Extracellular Matrix Proteins		
MYH9	Myosin Heavy Chain 9	226.32
COL4A1	Collagen Type IV Alpha 1 Chain	211.46
CTTN	Cortactin	202.50
DNHD1	Dynein heavy chain domain-containing protein 1	195.80
NEFL	Neurofilament light polypeptide	124.55
FLNA	Filamin-A	60.54
KIF5C	Kinesin heavy chain isoform 5C	60.34
TLN1	Talin-1	33.25
S100P	S100 Calcium Binding Protein P	21.23
SPTAN1	Spectrin alpha chain, non-erythrocytic 1	11.78
MYH11	Myosin Heavy Chain 11	8.99
DYNC1H1	Cytoplasmic dynein 1 heavy chain 1	8.51
COL1A1	Collagen Type I Alpha 1 Chain	7.38
CFL1	Cofilin-1	6.36
MYO18B	Myosin XVIIIB	6.11
PLEC1	Plectin 1, intermediate filament binding protein	5.48
SRRM2	Serine/arginine repetitive matrix protein 2	5.18
S100A16	S100 Calcium Binding Protein A16	4.87
SRRM1	Serine/arginine repetitive matrix protein 1	4.77
ACTN2	Alpha-actinin-2	4.31
MAP4	Microtubule-associated protein	4.22
DNM2	Dynamin-2	4.10
ARPC1B	Actin related protein 2/3 complex, subunit 1B	3.43
MACF1	Microtubule-actin cross-linking factor 1	3.26
VCL	Vinculin	2.66
TPM4	Tropomyosin alpha-4	2.65
ANKRD12	Ankyrin repeat domain-containing protein 12	2.58
VIL2	Villin 2 (Ezrin)	2.57
DYNC1LI2	Cytoplasmic dynein 1 light intermediate chain 2	2.42
VIM	Vimentin	2.37
NEFM	Neurofilament medium polypeptide	2.35
TUBB3	Tubulin beta-3	2.35
Senescence and the SASP (Senescence-Associated Secretory Phenotype)		
HMGB2	High mobility group protein B2	64.01
HMGB21	High mobility group protein B1	4.00
Autophagy/Lysosomal Markers		
ATP6V1E1	ATPase, H+ transporting, lysosomal, V1 subunit E1	2.60
ATP6V1A	V-type proton ATPase catalytic subunit A	2.56
CTSD	Cathepsin D	2.08

CTSZ	Cathepsin Z	2.07

-Proteins listed above were all upregulated in MCF7-Fibroblast Co-cultures ($p < 0.05$).